Reliability of dynamic network reconfiguration: Impact of code implementation, parameter selection, scan duration, and task condition

Zhen Yang[1,2*], Qawi K. Telesford[1], Alexandre R. Franco[1,3], Shi Gu[4], Ting Xu[3], Lei Ai[3], Ryan Lim[1], Francisco X. Castellanos[1,5], Chao-Gan Yan[6], Danielle S. Bassett[7,8], Stan Colcombe[1], Michael P. Milham[1,3*]

[1]Center for Biomedical Imaging and Neuromodulation, The Nathan S. Kline Institute for Psychiatric Research, Orangeburg, NY 10962 USA
[2]Department of Psychiatry, New York University, New York, NY 10016 USA
[3]Center for the Developing Brain, The Child Mind Institute, New York, NY 10022 USA
[4]University of Electronic Science and Technology of China, Chengdu, Sichuan, China
[5]Department of Child and Adolescent Psychiatry, Hassenfeld Children's Hospital at NYU Langone, New York, NY 10016 USA
[6]CAS Key Laboratory of Behavioral Science, Institute of Psychology, Beijing, China
[7]Departments of Bioengineering, Electrical & Systems Engineering, Physics & Astronomy, Psychiatry, Neurology, University of Pennsylvania, Philadelphia, PA 19104 USA;
[8]Santa Fe Institute, Santa Fe, NM 87501 USA

[*]Corresponding Author:

Zhen Yang PhD
Center for Biomedical Imaging and Neuromodulation
Nathan S. Kline Institute for Psychiatric Research
140 Old Orangeburg Rd, Orangeburg, NY 10962

Department of Psychiatry
New York University Grossman School of Medicine
550 1st Avenue, New York, NY 10016
E-mail: zhen.yang@nki.rfmh.org

Michael P. Milham, MD, PhD
Center for Biomedical Imaging and Neuromodulation
Nathan S. Kline Institute for Psychiatric Research
140 Old Orangeburg Rd, Orangeburg, NY 10962

Center for the Developing Brain
Child Mind Institute
101 East 56th Street, New York, NY 10022
E-mail: michael.milham@childmind.org

Keywords: reliability, multilayer networks, network dynamics, scan duration, naturalist viewing, individual differences

Highlights

Caution is needed when implementing the generalized Louvain community detection code.

We recommend optimizing multilayer network parameters using test-retest reliability.

Scan duration was a much stronger determinant of reliability than scan condition.

Minimal data need for movie condition is 20 min and for other conditions 30 min.

Combining different conditions improved test-retest reliability of dynamic estimates.

Abstract

Multilayer network models have been proposed as an effective means to capture the dynamic configuration of distributed neural circuits and quantitatively describe how communities vary over time. However, test-retest reliabilities for multilayer network measures are yet to be fully quantified. Here, we systematically evaluated the impact of code implementation, network parameter selections, scan duration, and task condition on test-retest reliability of key multilayer network measures (i.e., flexibility, integration, recruitment). We found that each of these factors impacted reliability, although to differing degrees. The choice of parameters is a longstanding difficulty of multilayer modularity-maximization algorithms. As suggested by prior work, we found that optimal parameter selection was a key determinant of reliability. However, due to changes in implementation of the multilayer community detection algorithm, our findings revealed a more complex story than previously appreciated, as the parameter landscape of reliability was found to be dependent on the implementation of the software.

Consistent with findings from the static functional connectivity literature, scan duration was found to be a much stronger determinant of reliability than scan condition. We found that both passive (i.e., resting state, Inscapes, and movie) and active (i.e., flanker) tasks can be highly reliable when the parameters are optimized and scan duration is sufficient, although reliability in the movie watching condition was significantly higher than in the other three tasks. Accordingly, the minimal data requirement for achieving reliable measures for the movie watching condition was 20 min, which is less than the 30 min needed for the other three tasks. Collectively, our results quantified test-retest reliability for multilayer network measures and support the utility of movie fMRI as a reliable context in which to investigate time-invariant network dynamics. Our practice of using test-retest reliability to optimize free parameters of multilayer modularity-maximization algorithms has the potential to enhance our ability to use these measures for the study of individual differences in cognitive traits.

1. Introduction

Following early seminal contributions (Watts and Strogatz 1998, Barabasi and Albert 1999), network science has played a pivotal role in revealing the structure and interactions of complex systems, such as social and transportation networks. More recently, this methodological approach has been applied to neuroscience, helping to further characterize the architecture of the human brain and launch the field of network neuroscience (Bullmore and Sporns 2009, Bassett and Sporns 2017). Accordingly, various tools have been developed to understand the brain as a complex network, highlighting variations in brain organization across development (Gu et al. 2015), aging (Voss et al. 2013), and clinical populations (Bassett et al. 2018). In many studies, brain networks are constructed from anatomic or functional neuroimaging data as a single network or static representation (Rubinov and Sporns 2010, Sporns 2013). As the human brain is intrinsically organized into functionally specialized modules, a common approach for analyzing brain networks is to investigate community structure, which identifies areas in the brain that are densely connected internally (Sporns and Betzel 2016). While this construction is useful, a growing literature suggests the brain, particularly its functional interactions, varies over time, thus necessitating the need to characterize these dynamic changes (Lurie et al. 2019)

Multilayer network models have been proposed as an effective means of capturing the temporal dependence between distributed neural circuits and of quantitatively describing how communities vary over time (Mucha et al. 2010, Kivela et al. 2014). Multilayer network models can be used to optimize the partitioning of nodes into modules by maximizing a multilayer modularity quality function that compares edge weights in an observed network to expected edge weights in a null network. In this approach, two parameters are essential: the intra-layer coupling parameter, which tunes the number of communities within a layer, and the inter-layer coupling parameter, which tunes the temporal dependence of communities detected across layers. Dynamic network measures derived from multilayer modularity include but are not limited to flexibility, recruitment, and integration. Flexibility quantifies how frequently a region changes its community membership over time (Bassett et al. 2011); recruitment can be defined as the probability that a region is assigned to its relevant cognitive system, such as that determined by an *a priori* atlas (e.g., visual, sensorimotor, and limbic systems); and integration can be defined as the probability that a region is *not* assigned to its relevant cognitive system (Bassett et al. 2015).

Initial applications of this approach have provided key insights into the brain network dynamics that underlie learning (Bassett et al. 2011, Bassett et al. 2015). Accordingly, there has been increased enthusiasm to utilize these methods in the neuroimaging field (**Table 1**). Specifically, these measures have been used to link network dynamics to inter-individual differences in a broad range of functional domains, including motor learning (Bassett et al. 2011, Wymbs et al. 2012, Bassett et al. 2015, Telesford et al. 2016), working memory (Braun et al. 2015), attention (Shine et al. 2016), language (Chai et al. 2016), mood (Betzel et al. 2017), creativity (Feng et al. 2019, He et al. 2019), and reinforcement learning (Gerraty et al. 2018). Additionally, dynamic network reconfiguration has been suggested as a potential biomarker for diseases, such as schizophrenia (Braun et al. 2016), temporal lobe epilepsy (He et al. 2018), and depression (Wei et al. 2017, Zheng et al. 2018, Shao et al. 2019), and has been used to predict antidepressant treatment outcome (Tian et al. 2019).

Despite these encouraging developments, there remain several open questions. First, it is unclear whether there are optimal parameter values for characterizing community structure dynamics, and the extent to which parameter choice may affect the reliability of findings. Second, the minimum data requirements to obtain reliable estimates for multilayer network-based measures have not been established. Previous studies vary in scan duration from 5 min to 3.45 hours (see **Table 1**). Third, how the choice of task during the scan (e.g., resting state, naturalistic viewing, or active tasks) impacts the reliability of dynamic network measurements obtained from multilayer modularity maximization has not been directly compared (Telesford et al. 2016). As dynamic brain network methods become more widespread, a systematic evaluation of the impact of these important factors on the test-retest reliability of multilayer network measures is important and timely (Nichols et al. 2017, Poldrack et al. 2017).

In this investigation, we aim to evaluate the impact of parameter selection, scan duration, and task condition on test-retest reliability of dynamic measures obtained from multilayer modularity maximization. We first identified the optimal intra-layer and inter-layer coupling parameters for the particular multilayer community detection algorithm that we employ, based on test-retest reliability. With the optimized parameters, we then evaluated test-retest reliability at various scan durations (i.e., 10, 20, 30, 40, 50, and 60 minutes) to determine the minimum data requirements for sufficient reliability. Given the growing popularity of naturalistic viewing, we examined reliability during Inscapes and movies, as well as resting-state and a flanker task to directly quantify the modulatory effect of mental states. Importantly, given recent updates to the options used to analyze dynamic community structure (Bazzi et al. 2016), we also evaluated the impact of software implementation on dynamic measurements and their test-retest reliability.

2. Material and methods

2. 1 Datasets

Our primary analysis included 10 adults who had minimal head motion (median framewise displacement within 1.5 interquartile range and ranged 0.04~0.08 mm) from the Healthy Brain

Network-Serial Scanning Initiative (HBN-SSI: http://fcon_1000.projects.nitrc.org/indi/hbn_ssi/): ages 23-37 years (29.8±5.3), 50% males. HBN-SSI is a project specifically designed for evaluating the test-retest reliability of functional connectivity measures during different task states. A detailed description of experimental design and data collection can be found in O'Connor et al. (2017). Briefly, each participant had 12 scanning sessions collected using the same imaging protocol over a 1~2-month period. At each session, a high-resolution structural image and four fMRI scans (i.e., resting state, Inscapes, movie, and flanker; 10 min/condition) were collected. All imaging data were collected using a 1.5T Siemens Avanto MRI scanner equipped with a 32- channel head coil in a mobile trailer (Medical Coaches, Oneonta, NY). Structural scans were collected for registration using a multi-echo MPRAGE sequence (TR=2.73 sec, echo time=1.64 ms, field of view=256×256 mm^2, voxel size=1.0×1.0 mm^3, flip angle=7°). fMRI scans were collected using a multiband echo planar imaging (EPI) sequence (multiband factor=3, TR=1.45 sec, echo time=40 ms, field of view=192×192 mm^2, voxel size=2.46×2.46×2.5 mm^3, flip angle=55°).

To test the impact of implementation choices in the multilayer community detection code, we created a toy multilayer network dataset and included resting-state fMRI data from 25 healthy adults from the Human Connectome Project (HCP) retest dataset (https://www.humanconnectome.org/study/hcp-young-adult/data-releases) (see **Supplementary Methods** for details on these datasets**)**. Furthermore, the generalizability of parameters optimized on the HBN-SSI dataset was evaluated on the HCP retest dataset.

2.2 Imaging preprocessing

Functional images were preprocessed using the Configurable Pipeline for the Analysis of Connectomes (C-PAC 1.3: http://fcp-indi.github.io/) with the following steps: (1) realignment to the mean EPI image to correct for motion; (2) nuisance signal regression: regressed out linear and quadratic trends, signals of five principal components derived from white matter and cerebrospinal fluid (Behzadi et al. 2007), global signal (Yang et al. 2014), and 24 common motion parameters (Friston et al. 1996); and (3) spatial normalization of functional data to Montreal Neurological Institute (MNI) space by combining boundary based registration (BBR) (Greve and Fischl 2009) and Advanced Normalization Tools (ANTs) (Avants et al. 2011).

2.3 Network construction

We defined nodes in the network using the functional parcellation from the CC200 atlas (Craddock et al. 2012) generated by a spatially constrained spectral clustering method. This functional parcellation consists of 200 ROIs covering the whole brain, each of which is homogeneous in its estimated functional connectivity. This commonly chosen atlas was previously used for studying static functional connectivity in the same dataset (O'Connor et al. 2017) and for evaluating reproducibility and reliability of state-based temporal dynamic methods (Yang et al. 2014). After preprocessing, we extracted mean signals from each ROI and then applied a sliding window to the time series. The window length (~100 s, 68 TRs, no overlap) was selected based on a previous multilayer network study (Telesford et al. 2016), which demonstrated that the number of communities stabilizes at a window length of ~100 s and inter-region variance of flexibility peaks at a window size of 75~120 s. Using a window length of ~100 s also allowed us to capture low frequency fluctuations with a low cutoff at 0.01 Hz.

For each window or layer, edges were estimated using wavelet coherence using the wavelet coherence toolbox (Grinsted et al., 2004: http://grinsted.github.io/wavelet-coherence/). As the most commonly used edge estimation for multilayer network analyses (**Table 1**), wavelet coherence is robust to outliers (Achard et al. 2006) and has advantages in terms of its utility for estimating correlations between fMRI time series, which display slowly decaying positive autocorrelations or long memory (Zhang et al. 2016, Telesford et al. 2017). Specifically, magnitude-squared coherence C_{xy} between a given pair of regions (x, y) is a function of the frequency (f) and defined by the equation:

$$C_{xy}(f) = \frac{\left|F_{xy}(f)\right|^2}{F_{xx}(f)F_{yy}(f)},$$

where $F_{xy}(f)$ is the cross-spectral density between region x and region y. The variables $F_{xx}(f)$ and $F_{yy}(f)$ are the autospectral densities of signals from region x and region y, respectively. The mean of $C_{xy}(f)$ over the frequency band of interest, in our case 0.01-0.10 Hz, is the edge weight between region x and region y. The range of wavelet coherence is bounded between 0 and 1. For each subject, we obtained a 200×200×6 (region×region×window) coherence matrix per task per session, which is coupled into a multilayer network by linking a node to itself in the preceding and the following windows or layers (Mucha et al. 2010, Bassett et al. 2011).

2.4 Dynamic community detection algorithm

A popular method for investigating community structure is to optimize the partitioning of nodes into modules such that a particularly chosen modularity quality function is maximized. Here, we used a Louvain-like locally greedy algorithm (Blondel et al. 2008) to maximize the multilayer modularity and partition brain regions into communities across layers (Mucha et al. 2010, Bassett et al. 2013a). This algorithm simultaneously assigns brain regions in all layers to communities so that community labels are consistent across layers, which avoids the common community matching problem. The multilayer modularity quality function (Q) is defined as:

$$Q = \frac{1}{2\mu}\sum_{ijlr}\{(A_{ijl} - \gamma_l M_{ijl})\delta_{lr} + \delta_{ij}\omega_{jlr}\}\left(\delta(g_{il}, g_{jr})\right)$$

where μ is the total edge weight; δ_{ij} is the Kronecker's δ-function that equals 1 when $i = j$ and 0 otherwise. The element A_{ijl} gives the strength of the edge between nodes *i* and *j* in layer l, and the element M_{ijl} is the corresponding edge expected in a null model. Here, we used the commonly used Newman-Girvan null model in which the element M_{ijl} is defined as

$$M_{ijl} = \frac{k_{il}k_{jl}}{2m_l},$$

where $m_l = \frac{1}{2}\sum_{ij} A_{ijl}$ is the total edge weight in layer l. The variables k_{il} and k_{jl} are the intra-layer strengths of node *i* and node *j* in layer l, respectively. In the quality function, g_{il} represents the community assignment of node *i* in layer l, and g_{jr} represents the community assignment of node *j* in layer *r*. Finally, $\delta(g_{il}, g_{jr}) = 1$ if $g_{il} = g_{jr}$ and $\delta(g_{il}, g_{jr}) = 0$ if $g_{il} \neq g_{jr}$.

When optimizing multilayer modularity, we must choose values for two parameters γ and ω. The parameter γ_l is the intra-layer coupling parameter for layer l, which defines how much weight we assign to the null network and controls the size of communities detected within layer l. The parameter ω_{jlr} is inter-layer coupling parameter which defines the weight of the inter-slice edges that link node *j* to itself between layer l and layer *r*. It controls the number of communities formed across layers. Here, these two parameters are assumed to be constant (γ_l=γ and ω_{jlr}=ω) across layers following previous work (**Table 1**). The choice of these two parameters is critical for multilayer modularity optimization, as they have a large impact on the detected community structure, as well as on the dynamic measures derived therefrom (Bassett et al. 2013a, Mattar et al. 2015, Chai et al. 2016). Multilayer modularity approaches were also shown to detect spurious group differences in dynamic network measures when these parameters were set inappropriately

(Lehmann et al. 2017). Here, we optimized these two parameters based on test-retest reliability. Specifically, we computed intra-class correlation coefficients (ICC) for each of the three dynamic network measures across a range of γ and a range of ω for each of the four tasks. Specifically, we considered the space spanned by the following ranges: γ=[0.95, 1.3] and ω=[0.1, 3.0]. We determined these ranges by applying the criterion that the number of modules be ≥2 and ≤100. As the space for γ is much smaller than that for ω, a smaller increment of 0.05 was used for γ and an increment of 0.1 was used for ω. After estimating the ICC at each point in this space, we identified the parameter value pair that produced the largest ICC. The γ and ω pair that produced the largest ICC the most frequently across the 12 conditions (3 dynamic network measures and 4 tasks) was chosen as the optimal one.

2.5. Implementation of a generalized Louvain (GenLouvain) algorithm

Dynamic community detection was performed using a generalized Louvain method for community detection implemented in MATLAB (Lucas et al. 2011-2019). In 2016, the code underwent a major revision that implemented a new randomization option to the function (Version 2.1). The new option, '*moverandw*', controls how a node is moved to form communities to optimize the quality function. When using the default option, '*move*' (choosing moves that result in maximal improvement in modularity), the algorithm exhibits an abrupt change in behavior when the inter-layer coupling parameter increases (see Bazzi et al. 2016 for more details). The newer option, '*moverandw*' (choosing moves at random from all moves that increase the quality where the probability of choosing a particular move is proportional to its increase in the quality function), mitigates these problems and tends to be better behaved for multilayer modularity with ordinal coupling. Thus, the new option was suggested by Bazzi et al. (2016) for multilayer network analysis. Given concerns regarding this abrupt behavior, we tested the impact of these two options on dynamic network measures and their test-retest reliabilities before implementing the code. We found the new option was superior in the aspects we tested (see Section 3.1 for details). Thus, the new option '*moverandw*' from the latest version of the code available when we started the project (Version 2.1.2) was used in the present work.

When implementing the GenLouvain method, we used fully weighted, unthresholded coherence matrices to minimize the known near degeneracy of the modularity landscape (Good et al. 2010). After applying this algorithm, the 200 ROIs were assigned to communities that span across layers. Due to the roughness of the modularity landscape (Good et al. 2010) and the stochastic nature of the algorithm (Blondel et al. 2008), the output of community detection often varies across optimizations. Thus, rather than focus on any single optimization, we computed the dynamic measures based on 100 optimizations, following the precedent of previous work (Bassett et al. 2011, Bassett et al. 2013a, Bassett et al. 2013b, Bassett et al. 2015). Specifically, we first calculated network measures (see next section for details) for each run of the community detection algorithm, and then we averaged those measures over the 100 optimizations.

2.6 Calculation of dynamic network measures

For each participant, we computed the following measures to characterize the dynamics of the multilayer network based on the dynamic community structure detected in each optimization.

2.6.1 Flexibility

For each brain region, the flexibility is calculated as the number of times a brain region changes its community assignment across layers, divided by the number of possible changes which is the number of layers minus 1 (Bassett et al. 2011). This measure characterizes a region's stability in community allegiance, and can be used to differentiate brain regions into a highly stable core and a highly flexible periphery (Bassett et al. 2013b). Regions with high flexibility are thought to have a larger tendency to interact with different networks. Average flexibility across the brain is also computed to examine the global flexibility of the system.

2.6.2 Module allegiance

The module allegiance matrix is the fraction of layers in which two nodes are assigned to the same community (Bassett et al. 2015). For each layer, a co-occurrence matrix (200×200) can be created based on the community assignment of each node pair. The element of the co-occurrence matrix is 1 if two nodes are assigned to the same community, and 0 otherwise. The module allegiance matrix is computed by averaging the co-occurrence matrices across layers, and the value of the matrix elements thus ranges from 0 to 1.

2.6.3 Integration and recruitment

To quantify the dynamic functional interactions among sets of brain regions located within pre-defined functional systems (i.e., seven networks defined by Yeo et al. 2011), we compute two network measures based on the module allegiance matrix: recruitment and integration (Bassett et al. 2015). Recruitment can measure the fraction of layers in which a region is assigned to the same community as other regions from the same pre-defined system. The recruitment of region i in system S is defined as:

$$R_i^S = \frac{1}{n_S} \sum_{j \in S} P_{ij} \, ,$$

where n_S is the number of regions in S, and P_{ij} is the module allegiance between node i and node j. The integration of region i with respect to system S is defined as:

$$I_i^S = \frac{1}{N - n_S} \sum_{j \notin S} P_{ij}$$

where N is the total number of brain regions. Integration I_i^S measures the fraction of layers in which region i is assigned to the same community as regions from systems other than S.

2.7 Assessment of reliability

Test-retest reliability and between-code reliability were assessed with the ICC estimated using the following linear mixed model:

$$Y_{ij}(v) = \mu_{00}(v) + \theta_{i0}(v) + \varepsilon_{ij}(v)\,,$$

where $Y_{ij}(v)$ represents the dynamic measure (i.e., flexibility, integration, or recruitment) for a given brain region v (v=1, 2…, 200), i indexes participants (i=1, 2, … 10), and j indexes either the session for analyses of test-retest reliability or the code implementation options for analyses of between-code reliability (j=1, 2). Further, $\mu_{00}(v)$ is the intercept or a fixed effect of the group average dynamic measure at region v; $\theta_{i0}(v)$ is the random effect for the i-th participant at region v; and $\varepsilon_{ij}(v)$ is the error term. The total variance of a given dynamic measure can be decomposed into two parts: (1) inter-individual variance across all participants (σ_θ^2=Var[θ]), and (2) intra-individual variance for a single participant across two measurements (σ_ε^2=Var[ε]). The reliability of each dynamic measure can then be calculated as:

$$ICC = \frac{\sigma_\theta^2}{\sigma_\theta^2 + \sigma_\varepsilon^2}\,.$$

The model estimations were implemented using the linear mixed effect (lme) function from the nlme R package (http://cran.r-project.org/web/packages/nlme).

2.8 Determination of the minimal data requirement

To establish minimal data requirements for sufficient test-retest reliability, we compared ICC values of the six scan durations: 10 min, 20 min, 30 min, 40 min, 50 min, and 60 min. Different scan durations were obtained by pseudo-randomly selecting 1, 2, 3, 4, 5, or 6 10-min sessions from 12 available sessions for each participant. Dynamic features were first computed for each of the 12 10-min sessions, and then averaged across the sessions that were selected for each scan duration. We did not compute the dynamic measures on concatenated time series data to avoid artifactually introducing community changes at the concatenation point. For each scan duration, ICC was estimated using linear mixed models. To increase the robustness of the results and to extract stable features, we repeated the analysis on 100 randomized samples for each duration. The same process was performed for each of the four tasks to determine the data necessary for each condition.

2.9 Determination of task dependency

To investigate how estimates of test-retest reliability might depend on task states, we first used hierarchical linear mixed models to assess between-condition and between-session reliability in the same model. Hierarchical linear mixed models separate the variations among task conditions (i.e., between-condition reliability) from variations between sessions (i.e., test-retest reliability) by estimating variance between participants, across the four task conditions (for the same participant), and between sessions within each condition (O'Connor et al. 2017). Our model took the following form:

$$Y_{ijk}(v) = \mu_{000}(v) + \theta_{jk}(v) + \phi_k(v) + \varepsilon_{ijk}(v)\,.$$

The dynamic measure for a given brain region v can be denoted as $Y_{ijk}(v)$, where i indexes over sessions, j indexes over conditions, and k indexes over participants. In this model, μ_{000} represents the intercept; θ_{jk} represents a random effect between sessions for the j-th condition of the k-th participant; ϕ_k represents a random effect for the k-th participant; and ε_{ijk} represents the error term. The variables $\theta_{jk}, \phi_k,$ and ε_{ijk} are assumed to be independent and to follow a normal distribution with zero mean. The total variances of a given dynamic measure can be decomposed into three parts: (1) variance between participants (σ_ϕ^2 = Var[ϕ]); (2) variance between conditions for the same participant (σ_θ^2= Var[θ]); and (3) variance of the residual, indicating variance between sessions (σ_ε^2 = Var[ε]). The reliability of each dynamic measure across conditions can be calculated as

$$ICC\ (conditions) = \frac{\sigma_\phi^2}{\sigma_\phi^2 + \sigma_\theta^2},$$

and across sessions as

$$ICC\ (sessions \mid conditions) = \frac{\sigma_\phi^2 + \sigma_\theta^2}{\sigma_\phi^2 + \sigma_\theta^2 + \sigma_\varepsilon^2}.$$

Next, we estimated the test-retest reliability for each task using the simple linear mixed models described in Section 2.7. The main effect of task condition on ICC values was tested using a nonparametric Friedman test. The Wilcoxon signed-rank test was used for *post hoc* analyses to determine which tasks differed significantly in test-retest reliability. As ICCs consistently increase with scan duration (Laumann et al. 2015, Xu et al. 2016, O'Connor et al. 2017), hierarchical and simple linear mixed models were performed using 60 minutes of data (the optimal scan duration in the current sample) to determine the impact of task condition.

3. Results

3.1 Impact of GenLouvain code implementation

In a previous study, when the old randomization option '*move*' of the GenLouvain code was used, an abrupt change in a quantitative measure computed from a multilayer output partition was observed in financial data (see Figure 5.4 of Bazzi et al. 2016). In our study, when the '*move*' option was used, we observed an apparent discontinuity in multilayer network-based dynamic measures in two independent human brain imaging datasets (HBN-SSI and HCP), as well as in a toy multilayer-network dataset (**Figure 1**). When the updated '*moverandw*' option was used, we no longer observed an apparent discontinuity. To evaluate reliability, we computed the ICC of flexibility between the two options. Consistent with our intuition, we found that most of the ICC values above the discontinuity were near zero, suggesting that flexibility values obtained using different randomization options are dramatically different in that portion of the parameter space. In addition to flexibility, we also investigated the impact of code implementation on integration and recruitment. We found that flexibility was the most impacted, integration was less impacted, and recruitment was the least impacted (**Figure S1**). Furthermore, we found that the newer '*moverandw*' option produced measures with greater test-retest reliability than the old '*move*' option (**Figure S2**), and better recovered known underlying dynamics in the toy data, especially in the portions of parameter space above the apparent discontinuity (See **Figure S3** and **S4** for details).

3.2 Parameter optimization based on test-retest reliability

Because our goal is to optimize multilayer network-derived measures to study individual differences, we chose our parameters based on test-retest reliability scores. We found that the selection of γ and ω had a large impact on the test-retest reliability of dynamic network measures (**Figure 2).** Depending on the parameter choice, test-retest reliability can range from low to high. Overall, recruitment (mean ICC across the landscape: 0.54±0.11) is more reliable than integration (0.37±0.17), and integration is more reliable than flexibility (0.30±0.15). For each measure, the pattern of ICC values across the 2-dimensional parameter space is highly similar across tasks. For

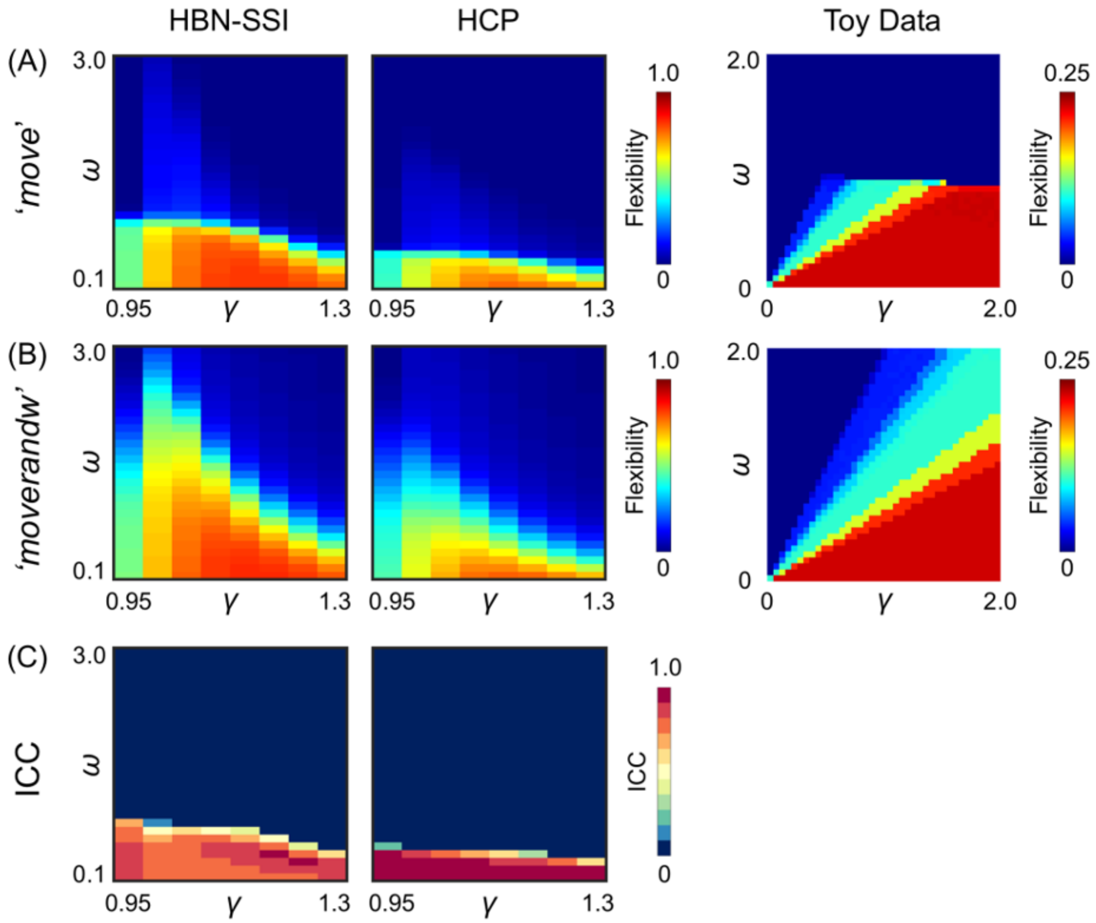

Figure 1. The impact of GenLouvain method ('*move*' vs '*moverandw*') on estimated values of flexibility. When the default option '*move*' was used (**A**), there was a drop-off in flexibility values in the 2-dimensional γ-ω parameter space. This apparent discontinuity was observed on flexibility values in two independent human brain imaging datasets, Healthy Brain Network-Serial Scanning Initiative (HBN-SSI) and Human Connectome Project (HCP), as well as in toy data. The issue was mitigated by the added option '*moverandw*' (**B**). Reliability between the two randomization options quantified using intra-class correlation coefficients (ICCs) was high before the apparent discontinuity and was near zero above the discontinuity (**C**). ICCs for HBN-SSI and HCP were evaluated based on 60 minutes of resting state data.

each task, the portions of the parameter space with high ICCs are consistent across measures. Thus, we were able to identify an optimal range of parameters generalizable across tasks and measures. For flexibility and integration, high ICCs (≥0.6) occur within a range of γ=[1.0-1.1] and ω=[1.7-3.0]. For recruitment, the range is broader: γ=[1.05-1.25] and ω=[1.2-3.0].

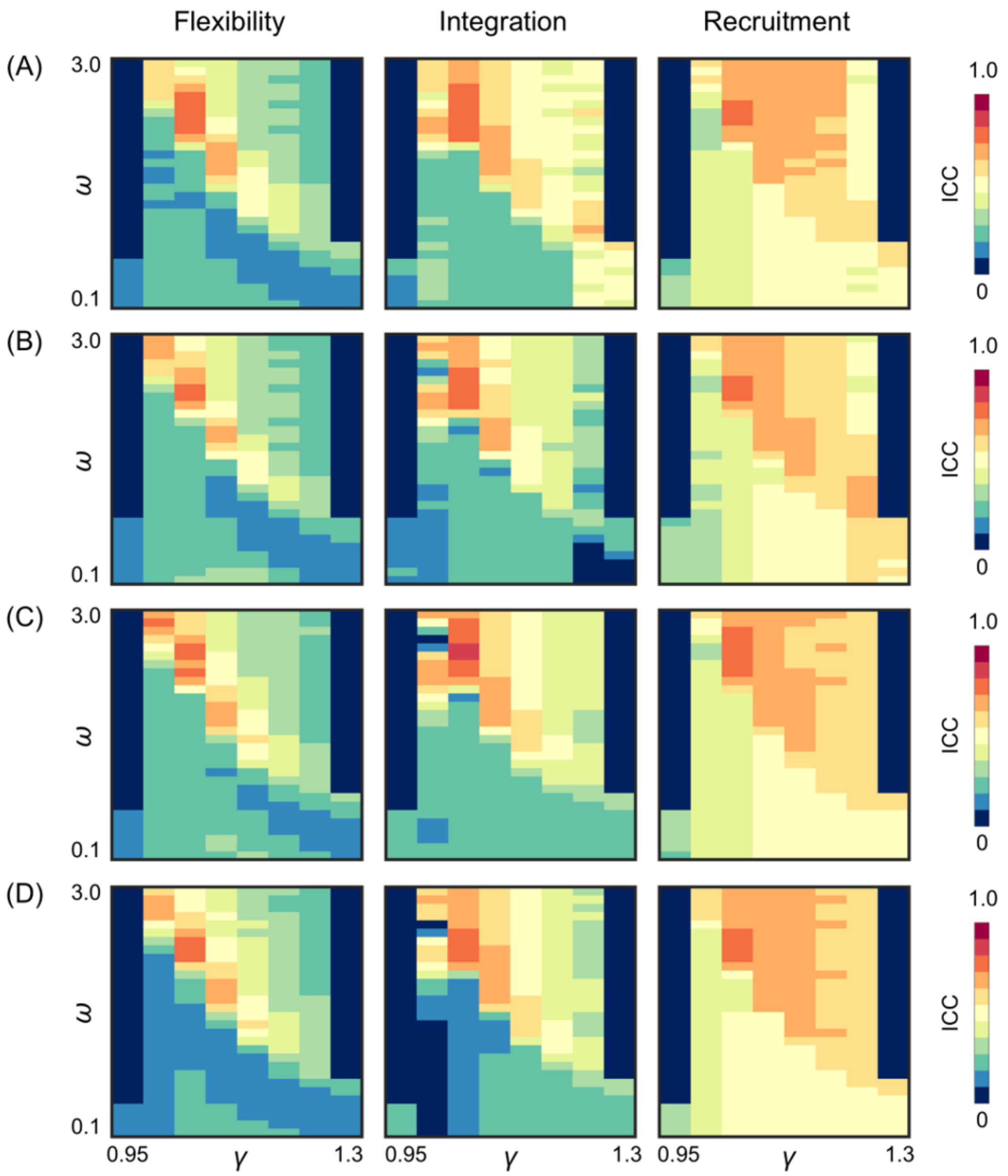

Figure 2. Test-retest reliability of dynamic network measures depends on the γ-ω selection. We identified a range of parameters that produced high test-retest reliability (ICC≥0.6) for each measure (flexibility, integration, and recruitment) and each task: (**A**) rest, (**B**) Inscapes, (**C**) movie, and (**D**) flanker. For a given measure, the mean ICC in the γ-ω plane computed across 200 ROIs was highly similar across tasks (compare rows). For a given task, the locations of high ICCs were highly consistent across measures (compare columns). The peak ICC value was observed in the same location (γ=1.05, ω=2.05) in 7 out of the 12 two-dimensional γ-ω planes. The ICC score at this location was also high (>0.65) in the other 5 two-dimensional γ-ω planes. Thus, this parameter value pair was chosen as the optimal γ-ω values for our analyses. Note that the values in the parameter space where the number of communities was smaller than 2 or greater than 100 were

set to zero in each plane. ICCs were evaluated with the maximal amount of data available (60 minutes).

For the current analysis, we chose the parameters γ=1.05 and ω=2.05, which produces maximal ICC values in 7 of the 12 γ-ω planes and still produces relatively high ICC values (ICC>0.65) in the other 5 γ-ω planes. Turning to the parameter ω which affects coupling between layers, tuning it up to 2.05 yielded low estimates of flexibility. In a previous study, when ω value was too high, flexibility values followed a heavy-tailed distribution with most values of flexibility equal to zero (i.e., close to a static network representation) (Telesford et al. 2016). In our investigation, the distribution of flexibility did not resemble this heavy-tailed distribution (**Figure S5A**), thus mitigating the potential concern that the parameter was tuned too high.

Because the ICC is determined by both within- and between-subject variability, high ICC could be caused by increased between-subject variability, decreased within-subject variability, or a combination of both. To understand the driver of this variation in test-retest reliability, we examined the landscape of dynamic measures, as well as the between- and within-subject variance of these dynamic measures. To make the variance values comparable, we normalized the between- and within-subject variance by the total variance. As expected, we found that the mean and variance of these dynamic measures also depended on the values chosen for γ and ω (**Figure 3**). The parameter values associated with high ICC overlapped with areas showing high between-subject variability and low within-subject variability, and largely overlapped with areas having relatively low values of the dynamic measures (integration has a few exceptions).

When the updated GenLouvain code that included '*moverandw*' was used, we found that reliability was low for the previously recommended and commonly used values of γ=1 and ω=1.

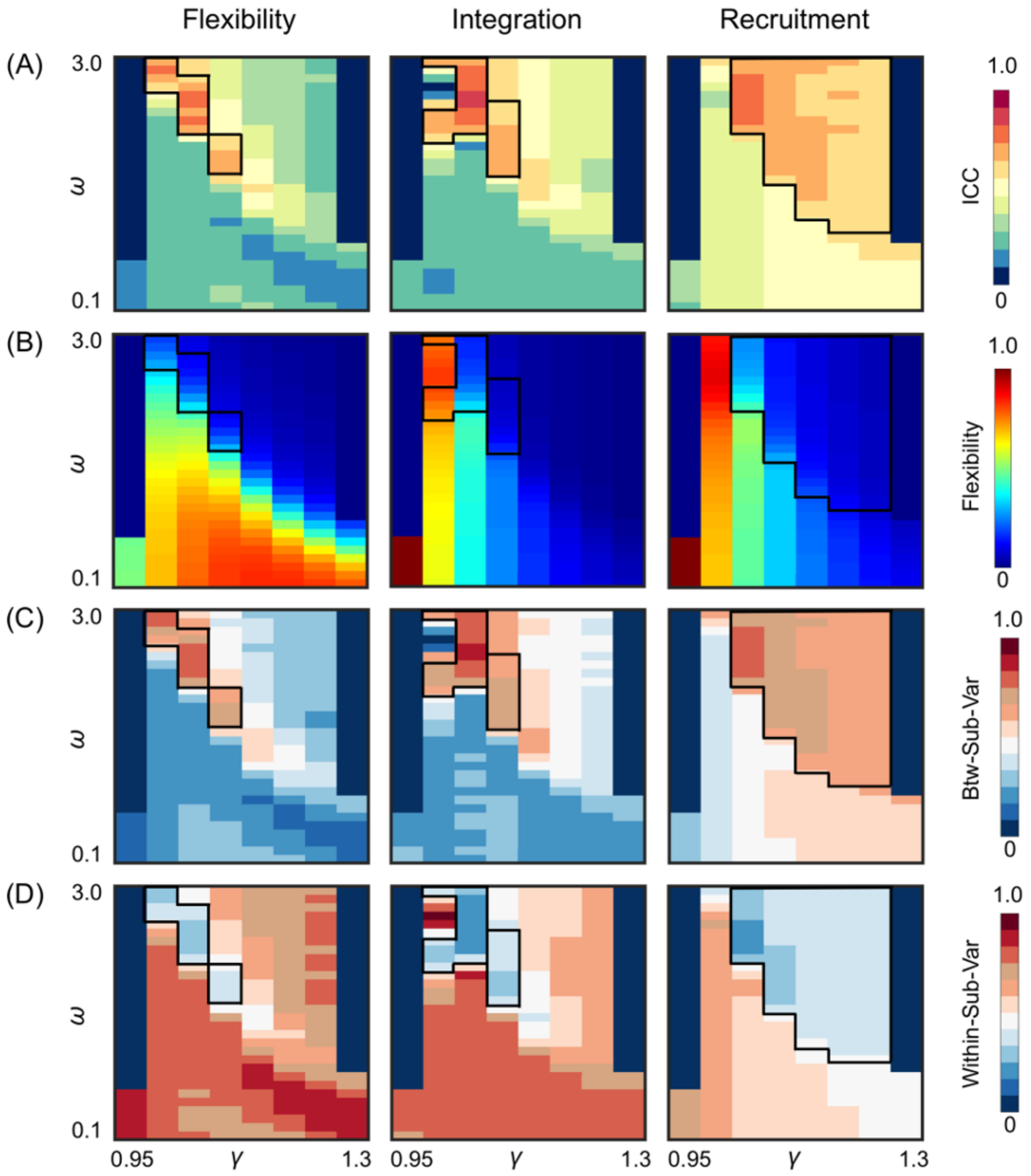

Figure 3. The portion of the γ-ω space with high ICCs (areas with ICC≥0.6 are indicated by black lines) overlapped largely with the portion with relatively low values of dynamic network measures (flexibility, integration, and recruitment), high between-subject variance, and low within-subject variance. **(A)** The ICC values for the same γ-ω plane specifically for the movie condition shown in Figure 2C; **(B)** The mean of the dynamic network measures computed across 200 ROIs; (**C**) Between-subject variance (Btw-Sub-Var); and (**D**) Within-subject variance (Within-Sub-Var).

To better understand this low reliability, we compared the recommended parameter choice with our reliability-optimized set. We found that although the spatial maps of flexibility were highly similar between two parameter choices (r=0.70), the magnitude of flexibility was much larger for [γ=1, ω=1] compared to [γ=1.05, ω=2.5]: 0.66±0.01 vs 0.16±0.01, respectively (**Figure S5A**). In the literature, when [γ=1, ω=1] was used, the range of flexibility is typically <0.25 (**Table 1**). This discrepancy is likely because early studies used a different randomization option of the GenLouvain code (the older '*move*' versus the newer '*moverandw*'). The low ICC of [γ=1, ω=1] (mean: 0.19±0.21) relative to [γ=1.05, ω=2.5] (mean: 0.79±0.08) when the new option was used was driven by the much lower between- and higher within-subject variance for [γ=1, ω=1] compared to [γ=1.05, ω=2.5] (except for the visual cortex).

To test the generalizability of our results, we applied the same multilayer analysis to HCP data and evaluated the test-retest reliability of flexibility. Compared to HBN-SSI data, we found that the areas with relatively high reliability were also located at the low γ and high ω areas for the HCP data, although flexibility values were lower for HCP in these areas. Importantly, we were unable to identify any parameter value pairs with an ICC≥0.6 for the HCP data, even though the overall reliability for the HCP data (mean ICC across the gamma-omega landscape: 0.27±0.03) is only slightly lower than that of the HBN-SSI data (mean: 0.30±0.15) (**Figure S6**). These results suggest that parameters optimized in one dataset may not be optimal for other datasets.

3.3 Data requirements for characterizing inter-individual differences in network dynamics

To establish the minimal data requirements for these types of analyses, we calculated the ICC for each measure and each task at six different scan durations: 10 min, 20 min, 30 min, 40 min, 50 min, and 60 min. Consistent with previous static analysis (Laumann et al. 2015, Xu et al. 2016, O'Connor et al. 2017), we found that test-retest reliability of dynamic measures improves with increased scan duration, and that this pattern is consistent across tasks and across dynamic network measures (**Figure 4**). From 10 to 60 min, the largest improvement is from 10 to 20 min. After 40 min, most regions achieved high ICCs and improvements were less notable for longer scan durations. For regional and system-level variations in improvement of reliability as a function of scan duration, see **Figure S7**.

Regarding the question of how much data is needed for sufficient reliability, the answer depends on the criteria, the task, and the measure. Here, we define good test-retest reliability as over 50% of ROIs with ICC≥0.5 (Xu et al. 2016). For the movie condition, good test-retest reliability was achieved for all three measures at 20 min (81.5% of ROIs had an ICC≥0.5 on average across all three measures) (**Figure 5**). For the flanker condition, good reliability was achieved at 20 min for integration (83.0% of ROIs ICC≥0.5) and recruitment (57.0% of ROIs ICC≥0.5). For the rest and Inscapes conditions, good reliability was achieved at 20 min only for integration (52.0% and 55.5% of ROIs ICC≥0.5, respectively). With 30 min of data, all measures and all tasks had good test-retest reliability. Across scan duration and task condition, integration is more reliable than recruitment (Wilcoxon signed-rank test: p<0.001) and recruitment is more reliable than flexibility (p=0.02).

When data for one task is insufficient, a potential solution is to combine different tasks to increase scan duration, and thus improve reliability (O'Connor et al. 2017, Elliott et al. 2019a). To test whether this approach is relevant to the types of analyses performed here, we compared the ICCs obtained from 10 min of resting state data with those obtained from longer data created by adding either more resting state data or data from the Inscapes, movie, and/or flanker task conditions. We found that increased scan duration was associated with improved reliability regardless of what tasks were combined (**Figure 6)**. Within each scan duration, the percent of ROIs with ICC>0.4 was comparable between mixed data and pure rest data (except for 20 min rest+movie and 30 min rest+movie+flanker), although the rest data alone had a larger percent of ROIs with high ICC (≥0.6).

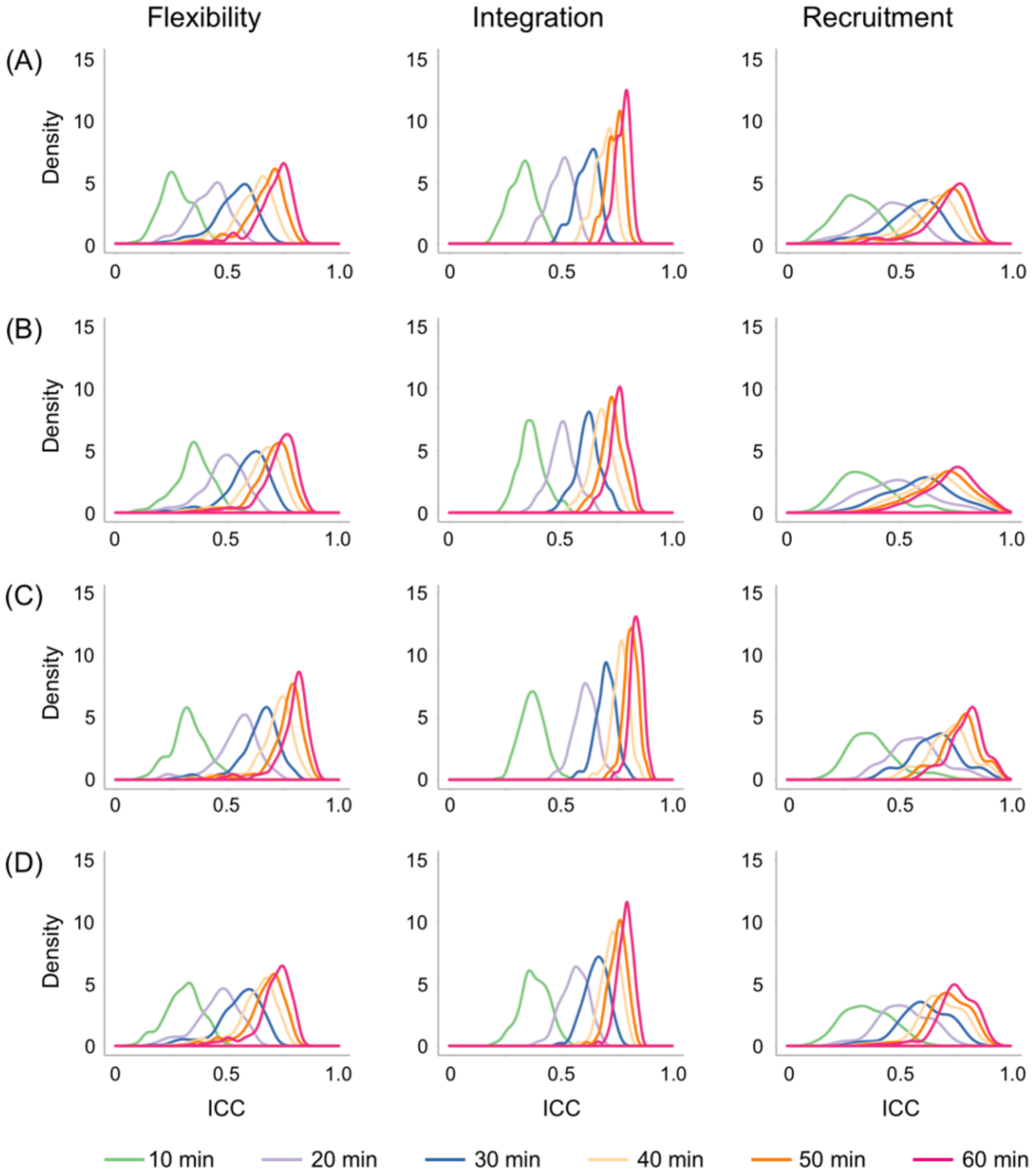

Figure 4. Test-retest reliability of dynamic network measures increases when the amount of data used for estimation increases. The density map of ICC values of 200 nodes were plotted for three dynamic measures (flexibility, integration, and recruitment) and four tasks (**A**: rest; **B**: Inscapes; **C**: movie; **D**: flanker) at six scan durations (10min, 20min, 30min, 40min, 50min, and 60min).

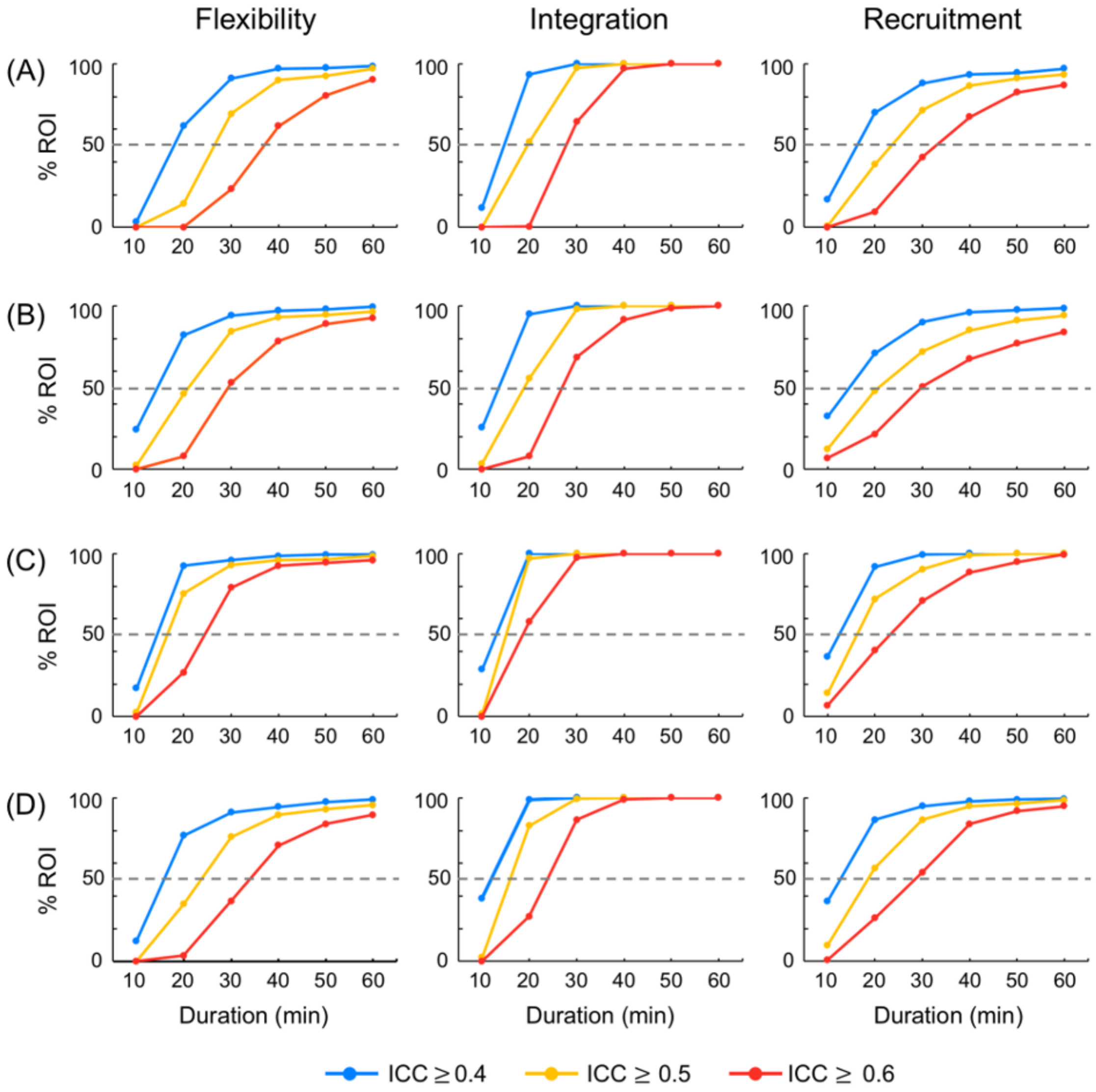

Figure 5. The minimal data requirements for sufficient reliability depending on the criteria, the measure, and the task. Percentage of ROIs with an ICC greater than 0.4 (blue line), 0.5 (orange line), and 0.6 (red line) were plotted for the three dynamic network measures (flexibility, integration, and recruitment) and the four tasks (**A**: rest; **B**: Inscapes; **C**: movie; **D**: flanker). The dashed grey line was drawn at 50%.

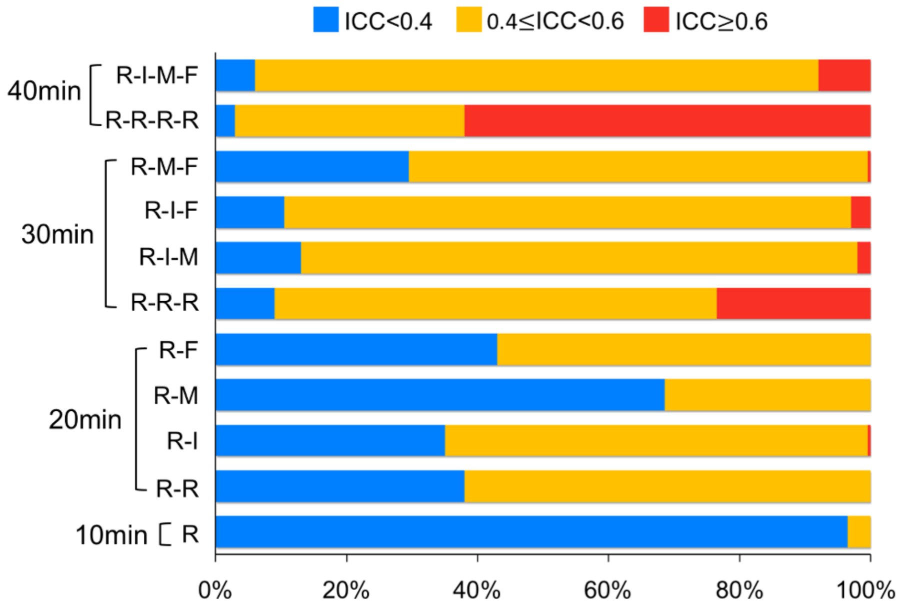

Figure 6. Combining data from different tasks improves reliability. Percent of ROIs showing low (blue: ICC<0.4), medium (orange: 0.4 ≤ ICC <0.6), or high (red: ICC≥0.6) reliability were plotted for four durations: 10 min, 20 min, 30min, and 40 min. For 10 min, the resting state data (R) were shown as a reference for comparison. For 20-40 min, the data were either pure R or a combination of R and the other three tasks: Inscapes (I), movie (M), and flanker (F). Each letter (the abbreviation of each condition) represents 10 min of data.

3.4 Task modulation on test-retest reliability of network dynamics: hierarchical linear mixed model

To separate variation among scan conditions from variations between sessions, we assessed between-condition reliability and between-session reliability simultaneously in a hierarchical linear mixed model. With the optimized γ-ω and the maximal amount of data available (60 min), we found that both between-session (two sessions, 60 min/session) and between-condition (four conditions) reliability were high (between-session median ± interquartile range: flexibility, 0.76±0.05; integration, 0.80±0.02; recruitment, 0.77±0.08; between-condition: flexibility, 0.74±0.10; integration, 0.76±0.07; recruitment, 0.77±0.16) (**Figure 7**). Consistent with previous work (O'Connor et al. 2017), we found that between-condition reliability of the visual and somatomotor network tended to be the lowest for recruitment which quantifies within-network functional interactions. Because different task states vary systematically in the richness of visual stimuli (movie>Inscapes>flanker>rest) and motor demands (flanker>the other three conditions), it is reasonable that these primary networks re-configure themselves according to unique task demands.

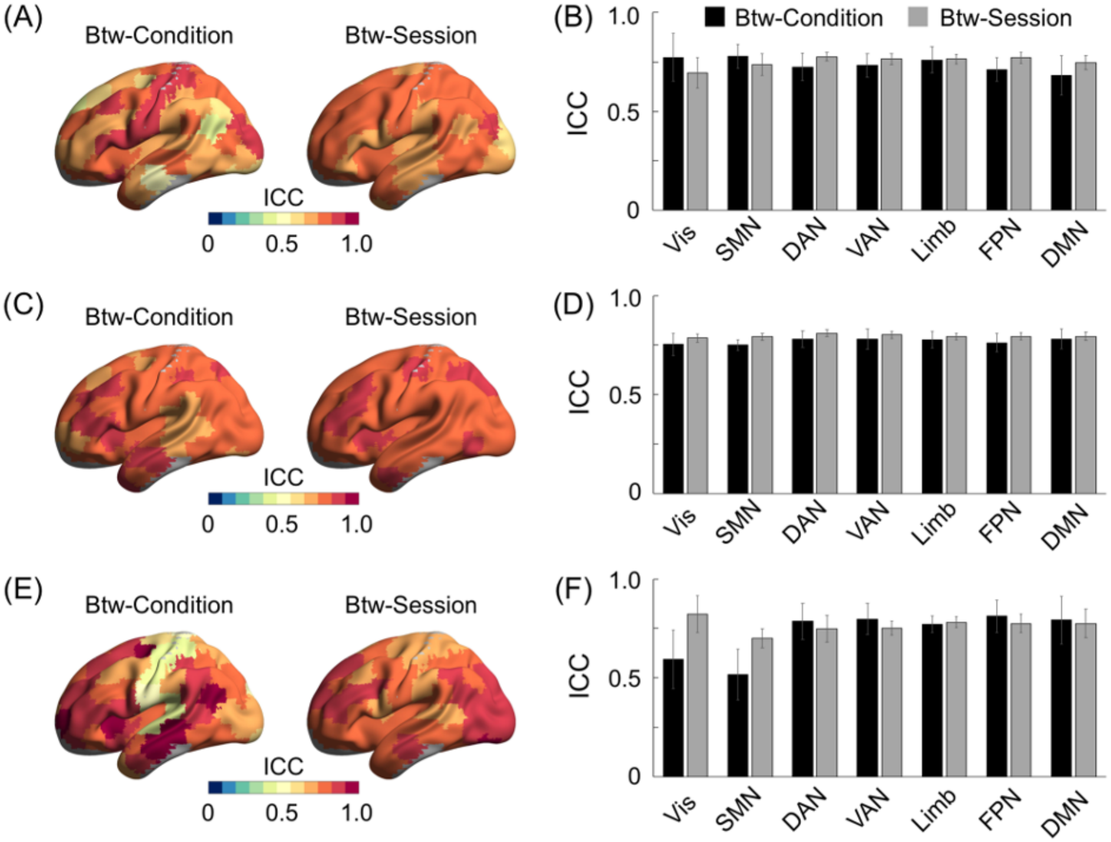

Figure 7. Both between-session and between-condition reliability evaluated in a hierarchical linear mixed model were high for 60 min of data. The between-condition (btw-condition: reliability between rest, Inscapes, movie, and flanker) and between-session (btw-session: reliability between test and retest) ICCs were plotted on the surface map using BrainNet Viewer (Xia et al. 2013) in Panel **A** (flexibility), **C** (integration), and **E** (recruitment), as well as summarized per the seven networks defined by Yeo et al. (2011) in bar plots in Panel **B** (flexibility), **D** (integration), and **F** (recruitment). Vis: visual network; SMN: somatomotor network; DAN: dorsal attention network; VAN: ventral attention network; Limb: limbic network; FPN: frontoparietal network: DMN: default mode network. The same network abbreviation was used for subsequent figures.

3.5 Task modulation on test-retest reliability of network dynamics: linear mixed model

Following the high-level model, we investigated test-retest reliability for each task separately using simple linear mixed models. We found that all four tasks have high test-retest reliability for all three measures (**Figure 8**). Median ± interquartile range of ICC for rest, Inscapes, movie, and flanker were: flexibility (0.73±0.09, 0.75±0.09, 0.81±0.07, 0.73±0.08), integration (0.78±0.05, 0.76±0.05, 0.84±0.04, 0.79±0.05), and recruitment (0.74±0.13, 0.74±0.16, 0.81±0.09, 0.76±0.11). When reliability was directly compared between tasks, there was a significant main effect of task for all three measures (Friedman test: p<0.001). Using *post hoc* testing, we found that the movie condition displayed significantly higher test-retest reliability in all dynamic network measures than the other three conditions (Wilcoxon signed-rank test: all p-values<0.001, below Bonferroni correction for 18 tests: 3 measures×6 possible pairing).

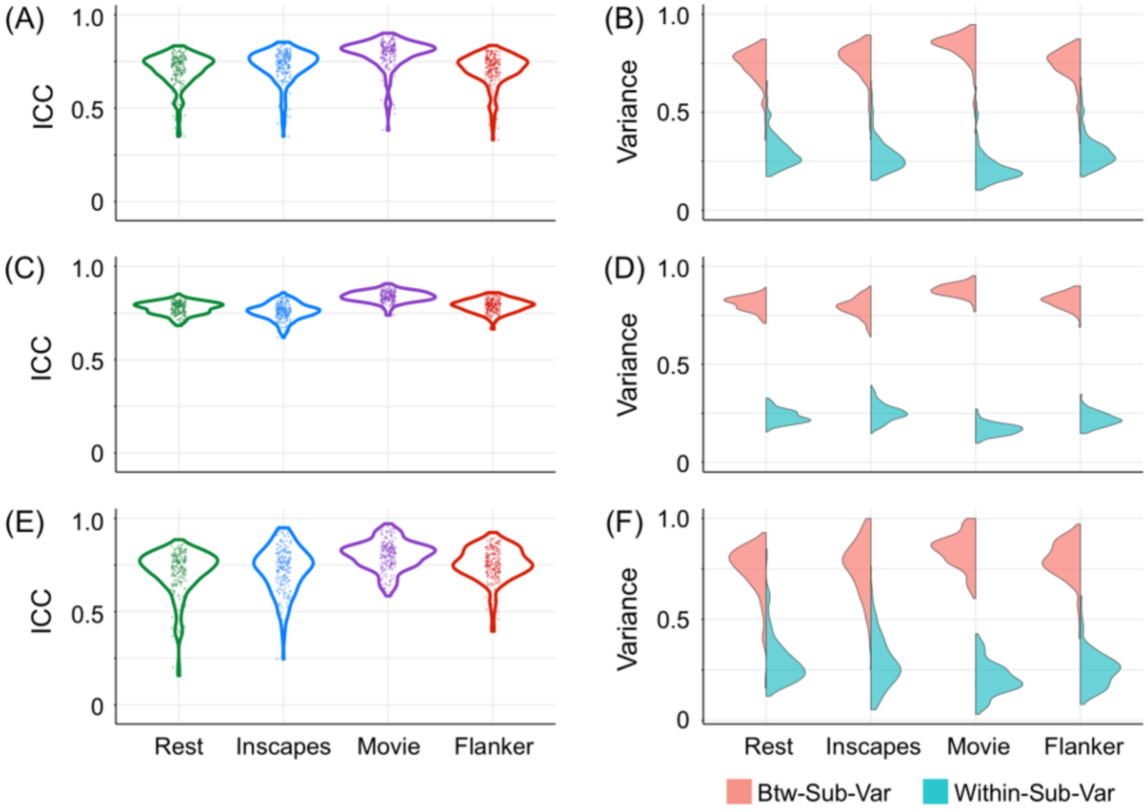

Figure 8. The movie condition was the most reliable condition. Distribution of ICCs of 200 ROIs were plotted for flexibility (**A**), integration (**C**), and recruitment (**E**) for four conditions (rest, Inscapes, movie, and flanker). Density of between-subject variance (btw-sub-var: salmon) and within-subject variance (within-sub-var: light sea green) were plotted for three dynamic measures (flexibility: **B**; integration: **D**; and recruitment: **F**) for each of the four conditions.

For the comparison of the remaining conditions, the results were measure dependent. For flexibility, test-retest reliability in the Inscapes condition was significantly higher than in the flanker condition (p<0.001, corrected), and the other comparisons were not significant; for integration, reliability differed significantly (flanker>rest>Inscapes, p<0.001, corrected); for recruitment, reliability in the flanker condition was also significantly higher than in the rest and Inscapes conditions (p<0.001, corrected). Generally, reliability of these dynamic measures did not simply increase as a function of task engagement. The higher ICC scores were typically associated with relatively higher between-subject variance and lower within-subject variance (**Figure 8**).

After considering overall reliability (median ICC), we next visualized regional and network differences in reliability between tasks. Consistent with overall results, we found that the movie condition exhibited higher reliability than the other three conditions in most brain regions and networks (**Figure 9**). The other three conditions are similar to each other with a few exceptions: flexibility of the somatomotor, visual, and default mode networks, and recruitment of the visual and somatomotor networks. The observation that task effects were most robust within the primary cortices is consistent with the hierarchical linear mixed model and with previous work (O'Connor et al. 2017).

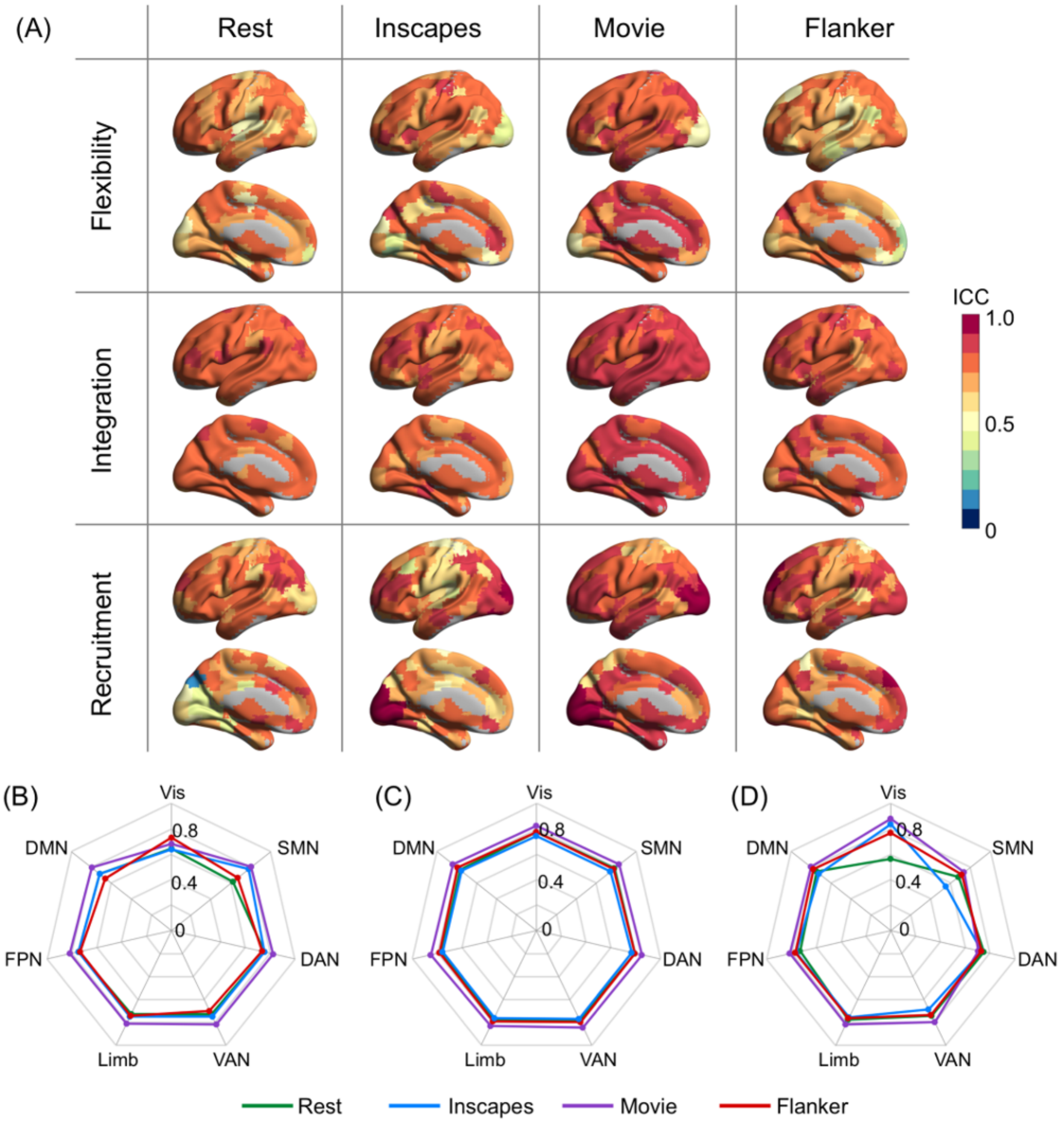

Figure 9. The impact of condition on test-retest reliability of dynamic network measures. **(A)** Spatial maps of ICCs for rest, Inscapes, movie, and flanker condition (columns) are shown on the brain surface for flexibility, integration, and recruitment (rows). ICCs of 200 ROIs were averaged based on Yeo et al. (2011)'s seven networks for each of the four conditions and shown in radar chart: flexibility (**B**), integration (**C**), and recruitment (**D**).

4. Discussion

Optimization of dynamic network methods for reliability is key to accurately characterizing trait-like individual differences in brain function. The present work examined the impact of code implementation, network parameter selection, scan duration, and task condition on the test-retest reliability of measures of dynamic community structure obtained using multilayer network models. We found that each of these factors impacted reliability, to differing degrees. As suggested by prior work, optimal parameter selection was found to be an important determinant of reliability; interestingly, our findings revealed a more complex story than previously appreciated, as reliability across the multivariate parameter space was found to be dependent on the version and the implementation of the software, due to a change in implementation of the multilayer community detection algorithm. Consistent with findings from the static functional connectivity literature, scan duration was found to be a much stronger determinant of reliability than scan condition. As is discussed in greater detail in the following sections, our findings suggest the value of continued optimization of multilayer network models before any single set of parameters or methods is accepted as standard practice.

4.1 A cautionary note on the version and implementation of GenLouvain code

In efforts to extract dynamic community structure from multilayer network models of data, many studies have capitalized on the generalized Louvain MATLAB community detection code (Lucas et al. 2011-2019). The earliest version of this code was developed for a paper describing the mathematical advances that allowed for community detection in multilayer networks (Mucha et al. 2010); the code was publicly released in 2011. Over the years, the code has been updated several times (Lucas et al. 2011-2019) to improve speed and enhance its applicability to multilayer settings. A previous study reported that when the default randomization option '*move*' was used, two computational issues arise: an under-emphasis of persistence and an abrupt drop in the number of intra-layer merges in certain portions of the parameter space, both of which can lead to an abrupt change in a quantitative measure derived (Bazzi et al. 2016). To address these problems, one randomization option '*moverand*' was added to the code in 2014 (Version 2.0) and another improved one '*moverandw*' was added in 2016 (Version 2.1). The fact that abrupt changes were observed consistently regardless of data type (previously observed in financial data and currently observed here in brain imaging data as well as in synthesized data), raises concerns regarding the accuracy of dynamic measures derived using the default option and with parameters selected above the point of apparent discontinuity in the 2-dimensional parameter space. Accordingly, we found that the between-code reliability for flexibility estimated in the affected areas of the parameter space were near zero, suggesting that the measures computed using the old and new GenLouvain options are not just a magnitude shift from one another but differ fundamentally. Based on these results, as well as our demonstration that '*moverandw*' has higher test-retest reliability and better validity compared to '*move*', we strongly recommend that investigators use '*moverandw*' for multilayer network analysis, especially when applied to ordinal or temporal networks.

4.2 Parameter optimization for multilayer network analyses

To detect community structures, we employed the most commonly used algorithm to maximize multilayer modularity quality function (Mucha et al. 2010). Communities that are detected using this algorithm are highly dependent on the free parameters (i.e., γ and ω), thus we aimed to explore the space defined by these parameters and identify optimal parameter selection ranges in terms of test-retest reliability. As one parameter may affect the other parameter's optimal setting, it can prove useful to optimize γ-ω jointly. Although several heuristics exist for choosing the "best" value of γ and ω (Bassett et al. 2013a, Chai et al. 2016, Weir et al. 2017), optimizing the ICC has not previously been proposed, possibly because it requires the acquisition of a retest dataset. Our results suggest that a systematic evaluation of the parameters in terms of reliability has marked utility, as parameter choices directly impact reliability.

In the 2-dimensional parameter space of the γ-ω plane, we were able to find a range of parameters that produced dynamic network measures of community structure in multilayer networks with high reliability. For flexibility and integration, higher reliability was achieved with higher ω (i.e., when there is a strong temporal coupling) and lower γ (i.e., when there are fewer communities). For recruitment, high reliability was achieved with high ω and a wide range of γ from low to high. Stronger temporal coupling in a multilayer network is typically associated with lower temporal variability in network partitions over time. The high test-retest reliability obtained at high ω and low γ, for flexibility and integration, may suggest that the temporal variability reserved after tuning up ω is composed of more between-subject variability than within-subject variability when the number of communities is small. The relative insensitivity of recruitment to the number of communities may be explained by our choice of predefined systems in which nodes tend to be grouped together over time. These results suggest that ICC-guided parameter selection can potentially maximize between-subject variability and minimize within-subject variability. This practice is consistent with the recent call for including assessment and optimization for reliability as a common practice in neuroimaging, as it helps to improve statistical power and decrease the amount of data required per subject (Zuo et al. 2019).

A critical cautionary note here is that the pattern of reliability across the 2-dimensional parameter space was also dependent on the version and implementation of the GenLouvain code. A parameter choice of [γ=1, ω=1] was recommended in the literature based on modularity and partition similarity, as well as the differences between measures estimated on a real network compared to an appropriate multilayer network null model (Bassett et al. 2013a). Following the initial work (Bassett et al. 2011, Bassett et al. 2013a), most studies have used [γ=1, ω=1] as their parameter choices (see **Table 1**) and tested the robustness of this parameter selection with small variations. As this parameter choice falls in the drop off area when the old GenLouvain code was used (**Figure 1 and Figure S1)** and it falls in the low test-retest reliability area when the updated GenLouvain code was used (**Figure S5**), the parameter choice of [γ=1, ω=1] needs to be reconsidered.

4.3 Minimal data requirements for obtaining reliable dynamic estimates

Many factors impact test-retest reliability of functional connectivity-based measures, among which scan duration is one of the most important (Zuo and Xing 2014, Zuo et al. 2019). Establishing minimal data requirements to obtain reliable estimates is an active research area for static connectivity analysis (Van Dijk et al. 2010, Anderson et al. 2011, Birn et al. 2013, Liao et al. 2013, Zuo et al. 2013, Laumann et al. 2015, Xu et al. 2016, Noble et al. 2017, Tomasi et al. 2017). However, to date, few efforts have been made to determine the scan duration needed to obtain reliable estimates of dynamic network measures. Here, we found that the test-retest reliability of dynamic network measures was poor for 10 min of data; it improved greatly when data increased to 20 min for movie fMRI and to 30 min for the other scan conditions. While increased scan duration has consistently been shown to improve reliability, studies vary in conclusions about the necessary data required to obtain reliable estimates. Studies have suggested that 5-10 min of data are sufficient to achieve respectable test-retest reliability (Van Dijk et al. 2010, Liao et al. 2013, Zuo et al. 2013, Tomasi et al. 2017); importantly, these studies have either focused on the default and frontoparietal networks, which have higher reliabilities than other functional networks, or used more complex derived measures than simple edge-wise complexity. More recent work has convergently reported a substantial improvement in reliability to a level more useful for characterizing trait-like individual differences when data are increased from 5-10 min to 20-30 min (Laumann et al. 2015, Xu et al. 2016, Noble et al. 2017, O'Connor et al. 2017, Elliott et al. 2019a). Our results are consistent with these static functional connectivity studies.

As temporal dynamic analyses are susceptible to spurious variations (Hutchison et al. 2013, Leonardi and Van De Ville 2015, Lehmann et al. 2017), one would assume more data are required to obtain reliable measures for dynamic analyses compared to static analyses. Instead, our data recommendations for estimating flexibility, recruitment, and integration from multilayer community detection analyses to examine trait-like individual differences are comparable to those for static functional connectivity analysis. This result may reflect our having optimized the analyses for test-retest reliability. As previous multilayer network-based studies vary widely in scan duration (ranging from 5 min to 3.45 hours: **Table 1**), it is crucial to establish minimal data requirements for the study of trait-like individual differences.

4.4 Improvement of test-retest reliability by combining different conditions

It may not be practical to collect 20 to 30 min of data for a single condition, which motivates the question of whether different conditions can be combined to increase scan duration and improve test-retest reliability. Our hierarchical linear mixed model revealed high between-condition reliability, as well as high between-session reliability. These results are consistent with previous static connectivity analysis using the HBN-SSI dataset which demonstrated high between-condition reliability (O'Connor et al. 2017). Our findings are also consistent with previous work showing that task and resting-state data share a large proportion of variance (Cole et al. 2014, Geerligs et al. 2015) and that inter-task variance was much smaller relative to inter-subject variance in functional connectivity (Finn et al. 2015, Gratton et al. 2018). Recent work leveraging shared features across resting-state and task fMRI using a method called 'general functional connectivity' have demonstrated that intrinsic connectivity estimated based on a combination of task and resting-state data offers better test-retest reliability than that estimated from the same amount of resting state data alone (Elliott et al. 2019a). Here, we also found that when scan duration was increased from 10 to 20, 30, or 40 min by combining task and resting-state data, the reliability of flexibility was greatly improved to a degree comparable to that estimated from 20, 30, or 40 min of resting data alone. Extending our understanding beyond prior studies of static connectivity, our results suggest dynamic network reconfiguration is similar across conditions when scan parameters and duration are optimized, thus supporting the feasibility of combining data from different tasks and conditions to improve reliability.

4.5 Movie fMRI identified as the most reliable condition

Another factor that impacts test-retest reliability of brain imaging-based measures is experimental paradigm due to the condition-dependent nature of brain activities (Zuo et al. 2019). Multilayer networks have been used to assess network reconfiguration during resting state (Mattar et al. 2015, Betzel et al. 2017, He et al. 2018), as well as during controlled cognitive tasks (Bassett et al. 2011, Bassett et al. 2015, Chai et al. 2016, Telesford et al. 2016, Gerraty et al. 2018). The present work extended previous work by including naturalistic viewing paradigms. Naturalistic paradigms offer increased ecological validity and allow studying highly interactive dynamic cognitive processes (Bottenhorn et al. 2019) and probing complex multimodal integration (Sonkusare et al. 2019). Thus, studies characterizing network dynamics and establishing test-retest reliability of these paradigms together have the potential to enhance our understanding of cognition as it occurs more naturally. A recent meta-analysis revealed that naturalistic paradigms recruit a common set of networks that allow separate processing of different streams of information as well as integration of relevant information to enable flexible cognitive and complex behavior (Bottenhorn et al. 2019).

Compared to a passive resting state and an active flanker condition, we found the movie condition had the highest test-retest reliability. These results are consistent with previous static network studies which suggested higher test-retest reliability for movie conditions when compared to resting state (Wang et al. 2017). Naturalistic viewing was shown to have enhanced ability to identify brain-behavioral correlations compared to conventional tasks (Cantlon and Li 2013, Vanderwal et al. 2019) and was less impacted by head motion (Vanderwal et al. 2015), especially for pediatric samples (Cantlon and Li 2013, Vanderwal et al. 2019). Some have suggested that the higher reliability may be explained by the enhanced ability of movie watching to detect inter-individual differences in functional connectivity that are unique at the individual level compared to resting state (Vanderwal et al. 2017); alternatively, findings might be related to the increased level of engagement for movies, which is known from the task fMRI to help stabilize connectivity patterns over time (Elton and Gao 2015). Regardless of explanation, the present results support the utility of naturalistic paradigms for investigating network dynamics in developmental and clinical applications.

4.6 Generalizability of the current findings to HCP data

We found that the test-retest reliability of the HCP data was much lower than that observed in the HBN-SSI dataset across the 2-dimensional γ-ω parameter space. One potential explanation is that HCP data were acquired using faster sampling than the HBN-SSI data (TR: 0.72 s vs. 1.45 s).

While static studies have indicated that increasing temporal resolution (Birn et al. 2013, Liao et al. 2013, Zuo et al. 2013) can improve reliability, the opposite was observed for dynamic analysis (Choe et al. 2017). Although the subjects in HCP and HBN-SSI are similar in terms of participant age and sex, the datasets differ in several acquisition and preprocessing parameters. Further work is needed to determine how to best optimize multilayer community detection measures accordingly.

Our results demonstrating that test-retest reliability can differ substantially between datasets suggest that parameters optimized in one dataset may not be optimal for others. Using test-retest reliability to optimize multilayer network analysis can facilitate reliable and efficient biomarker identification. However, challenges remain in terms of feasibility. The lack of generalizability may limit the application of this approach for datasets which do not have a retest sample. It is important for future studies to assess the generalizability of parameter optimization to datasets homogenized in key aspects of undesirable nonbiological source of variations, such as scanner manufacturer, acquisition protocol, and preprocessing steps. If such datasets are not available, applying statistical harmonization techniques, such as ComBat (i.e., combining batches) (Johnson et al. 2007, Fortin et al. 2018, Yu et al. 2018), could potentially remove unwanted site effects to optimize multilayer network analysis.

4.7 Addressing concerns regarding head motion

Head motion remains a major concern for dynamic functional connectivity estimation (Yang et al. 2014, Bassett et al. 2018, Satterthwaite et al. 2019). In the present work, we only included participants with minimal head motion. During preprocessing, we regressed out 24 motion-related parameters (Friston et al. 1996), as well as controlled motion with more generalized approaches such as global signal regression at the individual level (Yan et al. 2013, Yang et al. 2014, Lydon-

Staley et al. 2019a). To provide further insights into this concern, we examined the correlation with head motion, which we quantified as median framewise displacement (Jenkinson et al. 2002), and the global mean of each dynamic measure; we did not observe any significant correlations between these variables. Furthermore, we re-estimated test-retest reliability for flexibility on the movie condition using the optimized parameter while including median framewise displacement as a covariate at the group level in the linear mixed model. We found similarly high reliability with and without head motion included in the model (ICC=0.67 and 0.74, respectively), suggesting that the impact of head motion on test-retest reliability was small.

4.8 Limitations and future work

To estimate functional connectivity, we used wavelet coherence based on its predominance across similar studies in the literature (see **Table 1**), as well as due to its advantages in terms of denoising, robustness to outliers, and appropriateness for fMRI time series (Zhang et al. 2016). While wavelet coherence offers several advantages, it is a frequency-specific measure and does not utilize phase information (Percival and Walden 2000). As such, wavelet coherence is not useful when the phase of the signal is important. Ongoing work is examining the reliability of other connectivity estimation methods, such as the Pearson's correlation coefficient (Bassett et al. 2011, Mattar et al. 2015, Chai et al. 2016, Pedersen et al. 2018) which is informed by both phase and frequency information and which can be computed more swiftly. Future work should investigate how edge density and threshold, as well as edge weight sign (i.e., inclusion/exclusion of negative correlations) might impact the reliability of the dynamic network measures studied here.

We focused our analyses on low frequency fluctuations (0.01-0.1Hz). The lower reliability of the flanker condition compared to the movie condition could reflect our ignoring high frequency signals in the flanker task. To evaluate this possibility, we assessed flanker data reliability at a higher frequency range: 0.1-0.3 Hz. This range was selected to avoid the noisy upper bound (with TR=1.45 s, the highest frequency we can examine is 0.34 Hz). We found the reliability of dynamic measures obtained in the low frequency signals of the flanker task was much higher than in the higher frequency signals (**Figure S8**). This suggests that the low frequency signals carry more non-random between-subject variation for this task, and that the relatively low reliability of the flanker condition compared to the movie condition cannot be explained by frequency alone. Alternatively, the lower reliability of the flanker condition could be ascribed to its having been designed to minimize between-subject variance to "isolate" a single cognitive process (Elliott et al. 2019b).

We determined the size of the parameter space by considering the number of communities (≥2 and ≤100), and we estimated the ICC at each point in the 2-dimensional γ-ω parameter space at a relatively coarse scale (γ: 0.9-1.3 with increments of 0.05; ω: 0.1-3.0 with increments of 0.1). We note that this resolution is comparable to most previous work (Bassett et al. 2011, Bassett et al. 2013b, Braun et al. 2015, Braun et al. 2016, Chai et al. 2016, He et al. 2018). Recent extensions of the multilayer network approach to dynamic community detection have demonstrated that sweeping across a range of intra-coupling parameters can offer insights into the multi-scale hierarchical organization of the brain (Ashourvan et al. 2019). Moreover, such studies have demonstrated that inter- and intra-subject variability in modular structure are scale specific (Betzel et al. 2019). Thus, sampling community structure from more points in the γ, ω parameter space may provide a better characterization of the brain's dynamic network reconfiguration.

Indeed, some algorithms have been developed recently which allow a more refined and efficient search for parameters, for example, the Convex Hull of Admissible Modularity Partitions

(CHAMP) (Weir et al. 2017). Unlike the traditional way of selecting parameters in which the optimal partitions obtained at each (γ, ω) were treated independently, CHAMP uses the union of all computed partitions to identify the convex hull of a set of linear subspaces. It can greatly reduce the number of partitions that can be considered for future analyses by eliminating all partitions that were suboptimal across a given range of parameter space. Although the CHAMP software package is currently in its early versions (https://github.com/wweir827/CHAMP), future work implementing these methodological updates can potentially facilitate the parameter optimization process and map the ICC landscape in greater detail.

Optimization of multilayer network measures for reliability has the potential to enhance our ability to use these measures and study trait-like brain-behavior relationships more efficiently (Choe et al. 2017, Zuo et al. 2019). Establishing high reliability is a key component of reproducible research (Nichols et al. 2017, Poldrack et al. 2017). However, high test-retest reliability does not necessarily correspond to high sensitivity to detect brain-behavior relationships (Noble et al. 2017). Thus, it is important for future work to investigate the functional relevance of reliability-optimized dynamic network measures, as well as to consider optimizing the multilayer modularity framework based on other factors, such as discriminability between individuals (Bridgford et al. 2019) or predictive accuracy (Dadi et al. 2019). Prior work suggests that pipelines optimized on discriminability can better detect brain-phenotypic associations (Bridgford et al. 2019). Other prior work suggests that pipelines optimized on predictive accuracy give the best prediction for diverse targets (including neurodegenerative diseases, neuropsychiatric diseases, drug impact, and psychological traits) across multiple datasets (Dadi et al. 2019). Thus, adding these new dimensions as optimization targets may enhance the ability of multilayer network measures to become fundamental tools to delineate meaningful brain-behavior relationships. This approach may be particularly useful for examining developmental questions. Multi-layer network analyses have been applied to reveal developmental patterns in brain function (Betzel et al. 2015, Schlesinger et al. 2017b, Zhang et al. 2018). Changes in brain connectivity dynamics have also been reported in the context of other dynamic connectivity methods from childhood to adulthood (Faghiri et al. 2018, Vohryzek et al. 2019), during adolescence (Medaglia et al. 2018), and across the lifespan (Yan et al. 2017).

5. Conclusions

Here, we optimized the well-known multilayer modularity maximization framework for test-retest reliability and investigated the dependence of subsequent measures on modeling parameters, scan duration, and task condition. Our results provide evidence that dynamic measures from a common multilayer community detection technique (multilayer modularity maximization) can be highly reliable when the updated GenLouvain code was used, the parameters were optimized for reliability, and scan duration was sufficient. Although the movie condition was the most reliable, other passive (resting state and Inscapes) and active (flanker) conditions can be reliable as well when total scan duration is 30 minutes or longer. These results are promising and important, as there is a clear need in the network neuroscience field for reliable measures that can be used to find trait-like individual differences in cognition and diseases. Future work is needed to continue optimizing this framework by evaluating the impact of scanning parameters, preprocessing steps, and multilayer network analyses-related methodological decisions on reliability, as well as to optimize predictive accuracy.

Table 1. Summary of prior papers using flexibility, integration, or recruitment in the context of fMRI data.

Authors	**Task (Scan Duration)**	**Edge estimation**	γ	ω	**Flexibility Range**
Al-Sharoa et al. (2019)	Rest (8.8 min)	Pearson's correlation coefficient	1	1	N/A
Bassett et al. (2011)	Motor learning (3.45 hrs)	Pearson's correlation coefficient, wavelet coherence	1	1	<0.06
Bassett et al. (2013b)	Motor learning (3.45 hrs)	wavelet coherence	1	1	<0.20
Bassett et al. (2015)	Motor learning (3.45 hrs)	wavelet coherence	1	1	N/A
Betzel et al. (2017)	Rest (10 min/session, 91 sessions)	wavelet coherence	1	1	<0.25
Braun et al. (2015)	Working memory (~5 min)	wavelet coherence	1	1	<0.20
Braun et al. (2016)	Working memory (~5 min)	wavelet coherence	1	1	<0.15
Chai et al. (2016)	Semantic relatedness judgment Task (13 min) Story comprehension task (18~36 min)	Pearson's correlation coefficient	1	0.5	<0.20
Cole et al. (2014)	Dataset 1: Rest (10 min), Permuted rule operation cognitive task (72 min) Dataset 2 (HCP): Rest (56 min), 7 Tasks* (total 60 min)	Pearson's correlation coefficient	1	0-2	N/A
Cooper et al. (2019)	Persuasive messaging task (30.3 min)	wavelet coherence	N/A	N/A	<0.25
Feng et al. (2019)	Rest (~8 min)	Pearson's correlation coefficient	1	1	N/A
Gerraty et al. (2018)	Reinforcement learning (25 min)	wavelet coherence	1.18	1	<0.15
He et al. (2018)	Rest (5 min), Verbal generation task (5 min)	wavelet coherence	1	0.4	<0.25
He et al. (2019)	Rest (~8 min)	Pearson's correlation coefficient	1	1	N/A
Khambhati et al. (2018)	Rest (40 min)	multi-taper coherence	1	1	<0.20
Lehmann et al. (2017)	Simulated rest (12 min)	Pearson's correlation coefficient	1.25 1.5	2 1	N/A
Li et al. (2019)	Rest (~6.7 min)	wavelet correlation	1	1	<0.9
Lydon-Staley et al. (2019a)	Rest (6 min)	Pearson's correlation coefficient	1	1	<0.60
Lydon-Staley et al. (2019b)	Rest (6 min)	wavelet coherence	1	1	<0.60

Mattar et al. (2015)	Rest (10 min), Permuted rule operation cognitive task (72 min)	Pearson's correlation coefficient	1	0.45	N/A
Pedersen et al. (2018)	Rest (HCP: 60 min)	Pearson's correlation coefficient	1	1	<0.02
Schlesinger et al. (2017a)	Dataset 1: Recognition memory task (25.5 min) Dataset 2: Rest (6 min), attention task (20 min), memory task with lexical stimuli (22.5 min), face memory task (22.5 min)	wavelet coherence	1	1	Dataset 1: <0.55 Dataset 2: <0.5
Schlesinger et al. (2017b)	Word memory task (25.3 min)	wavelet coherence	1.2 1.15	0.05 0.001	<0.85
Shao et al. (2019)	Rest (6.75 min)	least absolute shrinkage and selection operator (LASSO)	1	1	N/A
Shine et al. (2016)	Rest (10 min/session, 84 sessions)	multiplication of temporal derivatives (MTD)	1	1	N/A
Telesford et al. (2016)	Recognition memory (20 min) Strategic attention task (20 min)	wavelet coherence	1	1	<0.25
Tian et al. (2019)	Rest (7 min)	Pearson's correlation coefficient	1	0.25	<0.045
Wei et al. (2017)	Rest (6.75 min)	conditional Granger causality	1	1	<0.65
Wymbs et al. (2012)	Motor learning (3.45 hrs)	Inter-key interval (IKI)	0.9	0.03	N/A
Zheng et al. (2018)	Rest (8 min)	Pearson's correlation coefficient	1	1	<0.2

Note: * 7 tasks from HCP are: emotional, gambling, language, motor, relational, social, and N-back task.

Acknowledgements

The work presented here was primarily supported by the NYS Office of Mental Health (AF, MPM, QT, SJC, ZY) and NIMH awards U01MH099059 (MPM), R24MH114806 (MPM), R01AG047596 (SJC, MPM), and R01MH111439 (MPM). Additional funding provided by gifts to the Child Mind Institute (CMI) from Phyllis Green and Randolph Cowen. We would also like to thank the many individuals who have provided financial support to the CMI Healthy Brain Network to make the creation and sharing of this resource possible. SG was supported by National Natural Science Foundation of China [NSFC-61876032]. CGY was supported by NSFC-81671774 and the Hundred Talents Program of the Chinese Academy of Sciences. Research was sponsored by the Army Research Office and was accomplished under Grant Number W911NF-18-1-0244 (DSB). The views and conclusions contained in this document are those of the authors and should not be interpreted as representing the official policies, either expressed or implied, of the Army Research Office or the U.S. Government. The U.S. Government is authorized to reproduce and distribute reprints for Government purposes notwithstanding any copyright notation herein. Data were provided in part by the Human Connectome Project, WU-Minn Consortium (Principal Investigators: David Van Essen and Kamil Ugurbil; 1U54MH091657) funded by the 16 NIH Institutes and Centers that support the NIH Blueprint for Neuroscience Research; and by the McDonnell Center for Systems Neuroscience at Washington University.

References

Achard, S., R. Salvador, B. Whitcher, J. Suckling and E. Bullmore (2006), "A resilient, low-frequency, small-world human brain functional network with highly connected association cortical hubs." *J Neurosci* **26**(1): 63-72.

Al-Sharoa, E., M. Al-Khassaweneh and S. Aviyente (2019), "Tensor Based Temporal and Multilayer Community Detection for Studying Brain Dynamics During Resting State fMRI." *IEEE Trans Biomed Eng* **66**(3): 695-709.

Anderson, J. S., M. A. Ferguson, M. Lopez-Larson and D. Yurgelun-Todd (2011), "Reproducibility of single-subject functional connectivity measurements." *AJNR Am J Neuroradiol* **32**(3): 548-555.

Ashourvan, A., Q. K. Telesford, T. Verstynen, J. M. Vettel and D. S. Bassett (2019), "Multi-scale detection of hierarchical community architecture in structural and functional brain networks." *PLoS One* **14**(5): e0215520.

Avants, B. B., N. J. Tustison, G. Song, P. A. Cook, A. Klein and J. C. Gee (2011), "A reproducible evaluation of ANTs similarity metric performance in brain image registration." *Neuroimage* **54**(3): 2033-2044.

Barabasi, A. L. and R. Albert (1999), "Emergence of scaling in random networks." *Science* **286**(5439): 509-512.

Bassett, D. S., M. A. Porter, N. F. Wymbs, S. T. Grafton, J. M. Carlson and P. J. Mucha (2013a), "Robust detection of dynamic community structure in networks." *Chaos* **23**(1): 013142.

Bassett, D. S. and O. Sporns (2017), "Network neuroscience." *Nat Neurosci* **20**(3): 353-364.

Bassett, D. S., N. F. Wymbs, M. A. Porter, P. J. Mucha, J. M. Carlson and S. T. Grafton (2011), "Dynamic reconfiguration of human brain networks during learning." *Proc Natl Acad Sci U S A* **108**(18): 7641-7646.

Bassett, D. S., N. F. Wymbs, M. P. Rombach, M. A. Porter, P. J. Mucha and S. T. Grafton (2013b), "Task-based core-periphery organization of human brain dynamics." *PLoS Comput Biol* **9**(9): e1003171.

Bassett, D. S., C. H. Xia and T. D. Satterthwaite (2018), "Understanding the Emergence of Neuropsychiatric Disorders With Network Neuroscience." *Biol Psychiatry Cogn Neurosci Neuroimaging* **3**(9): 742-753.

Bassett, D. S., M. Yang, N. F. Wymbs and S. T. Grafton (2015), "Learning-induced autonomy of sensorimotor systems." *Nat Neurosci* **18**(5): 744-751.

Bazzi, M., M. A. Porter, S. Williams, M. McDonald, D. J. Fenn and S. D. Howison (2016), "Community detection in termporal multilayer networks, with an application to correlation networks." *Multiscale Modeling Simul* **14**(1): 1-41.

Behzadi, Y., K. Restom, J. Liau and T. T. Liu (2007), "A component based noise correction method (CompCor) for BOLD and perfusion based fMRI." *Neuroimage* **37**(1): 90-101.

Betzel, R. F., M. A. Bertolero, E. M. Gordon, C. Gratton, N. U. F. Dosenbach and D. S. Bassett (2019), "The community structure of functional brain networks exhibits scale-specific patterns of inter- and intra-subject variability." *Neuroimage* **202**: 115990.

Betzel, R. F., B. Misic, Y. He, J. Rumschlag, X. N. Zuo and O. Sporns (2015), "Functional brain modules reconfigure at multiple scales across the human lifespan." *BioRxiv*.

Betzel, R. F., T. D. Satterthwaite, J. I. Gold and D. S. Bassett (2017), "Positive affect, surprise, and fatigue are correlates of network flexibility." *Sci Rep* **7**(1): 520.

Birn, R. M., E. K. Molloy, R. Patriat, T. Parker, T. B. Meier, G. R. Kirk, V. A. Nair, M. E. Meyerand and V. Prabhakaran (2013), "The effect of scan length on the reliability of resting-state fMRI connectivity estimates." *Neuroimage* **83**: 550-558.

Blondel, V. D., J. L. Guillaume, J. M. Hendrickx, C. de Kerchove and R. Lambiotte (2008), "Local leaders in random networks." *Phys Rev E Stat Nonlin Soft Matter Phys* **77**(3 Pt 2): 036114.

Bottenhorn, K. L., J. S. Flannery, E. R. Boeving, M. C. Riedel, S. B. Eickhoff, M. T. Sutherland and A. R. Laird (2019), "Cooperating yet distinct brain networks engaged during naturalistic paradigms: A meta-analysis of functional MRI results." *Netw Neurosci* **3**(1): 27-48.

Braun, U., A. Schafer, D. S. Bassett, F. Rausch, J. I. Schweiger, E. Bilek, S. Erk, N. Romanczuk-Seiferth, O. Grimm, L. S. Geiger, L. Haddad, K. Otto, S. Mohnke, A. Heinz, M. Zink, H. Walter, E. Schwarz, A. Meyer-Lindenberg and H. Tost (2016), "Dynamic brain network reconfiguration as a potential schizophrenia genetic risk mechanism modulated by NMDA receptor function." *Proc Natl Acad Sci U S A* **113**(44): 12568-12573.

Braun, U., A. Schafer, H. Walter, S. Erk, N. Romanczuk-Seiferth, L. Haddad, J. I. Schweiger, O. Grimm, A. Heinz, H. Tost, A. Meyer-Lindenberg and D. S. Bassett (2015), "Dynamic reconfiguration of frontal brain networks during executive cognition in humans." *Proc Natl Acad Sci U S A* **112**(37): 11678-11683.

Bridgford, E. W., S. Wang, Z. Yang, Z. Wang, T. Xu, R. C. Craddock, G. Kiar, W. Gray-Roncal, C. E. Priebe, B. Caffo, M. Milham, X. N. Zuo, C. f. R. a. Reproducibility and J. T. Vogelstein (2019), "Optimal experimental deisgn for big data: Applications in brain imaging." *BioRxiv*.

Bullmore, E. and O. Sporns (2009), "Complex brain networks: graph theoretical analysis of structural and functional systems." *Nat Rev Neurosci* **10**(3): 186-198.

Cantlon, J. F. and R. Li (2013), "Neural activity during natural viewing of Sesame Street statistically predicts test scores in early childhood." *PLoS Biol* **11**(1): e1001462.

Chai, L. R., M. G. Mattar, I. A. Blank, E. Fedorenko and D. S. Bassett (2016), "Functional Network Dynamics of the Language System." *Cereb Cortex* **26**(11): 4148-4159.

Choe, A. S., M. B. Nebel, A. D. Barber, J. R. Cohen, Y. Xu, J. J. Pekar, B. Caffo and M. A. Lindquist (2017), "Comparing test-retest reliability of dynamic functional connectivity methods." *Neuroimage* **158**: 155-175.

Cole, M. W., D. S. Bassett, J. D. Power, T. S. Braver and S. E. Petersen (2014), "Intrinsic and task-evoked network architectures of the human brain." *Neuron* **83**(1): 238-251.

Cooper, N., J. O. Garcia, S. H. Tompson, M. B. O'Donnell, E. B. Falk and J. M. Vettel (2019), "Time-evolving dynamics in brain networks forecast responses to health messaging." *Netw Neurosci* **3**(1): 138-156.

Craddock, R. C., G. A. James, P. E. Holtzheimer, 3rd, X. P. Hu and H. S. Mayberg (2012), "A whole brain fMRI atlas generated via spatially constrained spectral clustering." *Hum Brain Mapp* **33**(8): 1914-1928.

Dadi, K., M. Rahim, A. Abraham, D. Chyzhyk, M. Milham, B. Thirion, G. Varoquaux and I. Alzheimer's Disease Neuroimaging (2019), "Benchmarking functional connectome-based predictive models for resting-state fMRI." *Neuroimage* **192**: 115-134.

Elliott, M. L., A. R. Knodt, M. Cooke, M. J. Kim, T. R. Melzer, R. Keenan, D. Ireland, S. Ramrakha, R. Poulton, A. Caspi, T. E. Moffitt and A. R. Hariri (2019a), "General functional connectivity: Shared features of resting-state and task fMRI drive reliable and heritable individual differences in functional brain networks." *Neuroimage* **189**: 516-532.

Elliott, M. L., A. R. Knodt, D. Ireland, M. L. Morris, R. Poulton, S. Ramrakha, M. L. Sison, T. E. Moffitt, A. Caspi and A. R. Hariri (2019b), "Poor test-retest reliability of task-fMRI: New empirical evidence and a meta-analysis." *BioRxiv*.

Elton, A. and W. Gao (2015), "Task-related modulation of functional connectivity variability and its behavioral correlations." *Hum Brain Mapp* **36**(8): 3260-3272.

Faghiri, A., J. M. Stephen, Y. P. Wang, T. W. Wilson and V. D. Calhoun (2018), "Changing brain connectivity dynamics: From early childhood to adulthood." *Hum Brain Mapp* **39**(3): 1108-1117.

Feng, Q., L. He, W. Yang, Y. Zhang, X. Wu and J. Qiu (2019), "Verbal Creativity Is Correlated With the Dynamic Reconfiguration of Brain Networks in the Resting State." *Front Psychol* **10**: 894.

Finn, E. S., X. Shen, D. Scheinost, M. D. Rosenberg, J. Huang, M. M. Chun, X. Papademetris and R. T. Constable (2015), "Functional connectome fingerprinting: identifying individuals using patterns of brain connectivity." *Nat Neurosci* **18**(11): 1664-1671.

Fortin, J. P., N. Cullen, Y. I. Sheline, W. D. Taylor, I. Aselcioglu, P. A. Cook, P. Adams, C. Cooper, M. Fava, P. J. McGrath, M. McInnis, M. L. Phillips, M. H. Trivedi, M. M. Weissman and R. T. Shinohara (2018), "Harmonization of cortical thickness measurements across scanners and sites." *Neuroimage* **167**: 104-120.

Friston, K. J., S. Williams, R. Howard, R. S. Frackowiak and R. Turner (1996), "Movement-related effects in fMRI time-series." *Magn Reson Med* **35**(3): 346-355.

Geerligs, L., M. Rubinov, C. Cam and R. N. Henson (2015), "State and Trait Components of Functional Connectivity: Individual Differences Vary with Mental State." *J Neurosci* **35**(41): 13949-13961.

Gerraty, R. T., J. Y. Davidow, K. Foerde, A. Galvan, D. S. Bassett and D. Shohamy (2018), "Dynamic Flexibility in Striatal-Cortical Circuits Supports Reinforcement Learning." *J Neurosci* **38**(10): 2442-2453.

Good, B. H., Y. A. de Montjoye and A. Clauset (2010), "Performance of modularity maximization in practical contexts." *Phys Rev E Stat Nonlin Soft Matter Phys* **81**(4 Pt 2): 046106.

Gratton, C., T. O. Laumann, A. N. Nielsen, D. J. Greene, E. M. Gordon, A. W. Gilmore, S. M. Nelson, R. S. Coalson, A. Z. Snyder, B. L. Schlaggar, N. U. F. Dosenbach and S. E. Petersen (2018), "Functional Brain Networks Are Dominated by Stable Group and Individual Factors, Not Cognitive or Daily Variation." *Neuron* **98**(2): 439-452 e435.

Greve, D. N. and B. Fischl (2009), "Accurate and robust brain image alignment using boundary-based registration." *Neuroimage* **48**(1): 63-72.

Grinsted, A., J.C. Moore, S.Jevrejeva (2004), "Application of the cross wavelet transform and wavelet coherence to geophysical time series. *Nonlinear Processes Geophys* 11(5/6): 561-566.

Gu, S., T. D. Satterthwaite, J. D. Medaglia, M. Yang, R. E. Gur, R. C. Gur and D. S. Bassett (2015), "Emergence of system roles in normative neurodevelopment." *Proc Natl Acad Sci U S A* **112**(44): 13681-13686.

He, L., K. Zhuang, Y. Li, J. Sun, J. Meng, W. Zhu, Y. Mao, Q. Chen, X. Chen and J. Qiu (2019), "Brain flexibility associated with need for cognition contributes to creative achievement." *Psychophysiology* **56**(12): e13464.

He, X., D. S. Bassett, G. Chaitanya, M. R. Sperling, L. Kozlowski and J. I. Tracy (2018), "Disrupted dynamic network reconfiguration of the language system in temporal lobe epilepsy." *Brain* **141**(5): 1375-1389.

Hutchison, R. M., T. Womelsdorf, E. A. Allen, P. A. Bandettini, V. D. Calhoun, M. Corbetta, S. Della Penna, J. H. Duyn, G. H. Glover, J. Gonzalez-Castillo, D. A. Handwerker, S. Keilholz, V. Kiviniemi, D. A. Leopold, F. de Pasquale, O. Sporns, M. Walter and C. Chang (2013), "Dynamic functional connectivity: promise, issues, and interpretations." *Neuroimage* **80**: 360-378.

Jenkinson, M., P. Bannister, M. Brady and S. Smith (2002), "Improved optimization for the robust and accurate linear registration and motion correction of brain images." *Neuroimage* **17**(2): 825-841.

Johnson, W. E., C. Li and A. Rabinovic (2007), "Adjusting batch effects in microarray expression data using empirical Bayes methods." *Biostatistics* **8**(1): 118-127.

Khambhati, A. N., M. G. Mattar, N. F. Wymbs, S. T. Grafton and D. S. Bassett (2018), "Beyond modularity: Fine-scale mechanisms and rules for brain network reconfiguration." *Neuroimage* **166**: 385-399.

Kivela, M., A. Arenas, M. Barthelemy, J. P. Gleeson, Y. Moreno and M. A. Porter (2014), "Multilayer networks." *J Complex Netw*(2): 203-271.

Laumann, T. O., E. M. Gordon, B. Adeyemo, A. Z. Snyder, S. J. Joo, M. Y. Chen, A. W. Gilmore, K. B. McDermott, S. M. Nelson, N. U. Dosenbach, B. L. Schlaggar, J. A. Mumford, R. A. Poldrack and S. E. Petersen (2015), "Functional System and Areal Organization of a Highly Sampled Individual Human Brain." *Neuron* **87**(3): 657-670.

Lehmann, B. C. L., S. R. White, R. N. Henson, C. Cam and L. Geerligs (2017), "Assessing dynamic functional connectivity in heterogeneous samples." *Neuroimage* **157**: 635-647.

Leonardi, N. and D. Van De Ville (2015), "On spurious and real fluctuations of dynamic functional connectivity during rest." *Neuroimage* **104**: 430-436.

Li, Q., X. Wang, S. Wang, Y. Xie, X. Li, Y. Xie and S. Li (2019), "Dynamic reconfiguration of the functional brain network after musical training in young adults." *Brain Struct Funct* **224**(5): 1781-1795.

Liao, X. H., M. R. Xia, T. Xu, Z. J. Dai, X. Y. Cao, H. J. Niu, X. N. Zuo, Y. F. Zang and Y. He (2013), "Functional brain hubs and their test-retest reliability: a multiband resting-state functional MRI study." *Neuroimage* **83**: 969-982.

Lucas, G. S., J. M. Bazzi, I. S. Jutla and P. J. Mucha (2011-2019), "A generalized Louvain method for community detection implemented in MATLAB."

Lurie, D. J., D. Kessler, D. S. Bassett, R. F. Betzel, M. Breakspear, S. Keilholz, A. Kucyi, R. Liegeois, M. A. Lindquist, A. R. McIntosh, R. A. Poldrack, J. M. Shine, W. H. Thompson, N. Z. Bielezyk, L. Douw, D. Kraft, R. L. Miller, M. Muthuraman, L. Pasquini, A. Razi, D. Vidaurre, H. Xie and V. D. Calhoun (2019), "Questions and controversies in the study of time-varying functional connectivity in resting fMRI." *Network Neuroscience*.

Lydon-Staley, D. M., R. Ciric, T. D. Satterthwaite and D. S. Bassett (2019a), "Evaluation of confound regression strategies for the mitigation of micromovement artifact in studies of dynamic resting-state functional connectivity and multilayer network modularity." *Network Neuroscience* **3**(2): 427-454.

Lydon-Staley, D. M., C. Kuehner, V. Zamoscik, S. Huffziger, P. Kirsch and D. S. Bassett (2019b), "Repetitive negative thinking in daily life and functional connectivity among default mode, fronto-parietal, and salience networks." *Transl Psychiatry* **9**(1): 234.

Mattar, M. G., M. W. Cole, S. L. Thompson-Schill and D. S. Bassett (2015), "A Functional Cartography of Cognitive Systems." *PLoS Comput Biol* **11**(12): e1004533.

Medaglia, J. D., T. D. Satterthwaite, A. Kelkar, R. Ciric, T. M. Moore, K. Ruparel, R. C. Gur, R. E. Gur and D. S. Bassett (2018), "Brain state expression and transitions are related to complex executive cognition in normative neurodevelopment." *Neuroimage* **166**: 293-306.

Mucha, P. J., T. Richardson, K. Macon, M. A. Porter and J. P. Onnela (2010), "Community structure in time-dependent, multiscale, and multiplex networks." *Science* **328**(5980): 876-878.

Nichols, T. E., S. Das, S. B. Eickhoff, A. C. Evans, T. Glatard, M. Hanke, N. Kriegeskorte, M. P. Milham, R. A. Poldrack, J. B. Poline, E. Proal, B. Thirion, D. C. Van Essen, T. White and B. T.

Yeo (2017), "Best practices in data analysis and sharing in neuroimaging using MRI." *Nat Neurosci* **20**(3): 299-303.

Noble, S., M. N. Spann, F. Tokoglu, X. Shen, R. T. Constable and D. Scheinost (2017), "Influences on the Test-Retest Reliability of Functional Connectivity MRI and its Relationship with Behavioral Utility." *Cereb Cortex* **27**(11): 5415-5429.

O'Connor, D., N. V. Potler, M. Kovacs, T. Xu, L. Ai, J. Pellman, T. Vanderwal, L. C. Parra, S. Cohen, S. Ghosh, J. Escalera, N. Grant-Villegas, Y. Osman, A. Bui, R. C. Craddock and M. P. Milham (2017), "The Healthy Brain Network Serial Scanning Initiative: a resource for evaluating inter-individual differences and their reliabilities across scan conditions and sessions." *Gigascience* **6**(2): 1-14.

Pedersen, M., A. Zalesky, A. Omidvarnia and G. D. Jackson (2018), "Multilayer network switching rate predicts brain performance." *Proc Natl Acad Sci U S A* **115**(52): 13376-13381.

Percival, D. B. and A. T. Walden (2000). Wavelet methods for time series analysis, Cambridge University Press.

Poldrack, R. A., C. I. Baker, J. Durnez, K. J. Gorgolewski, P. M. Matthews, M. R. Munafo, T. E. Nichols, J. B. Poline, E. Vul and T. Yarkoni (2017), "Scanning the horizon: towards transparent and reproducible neuroimaging research." *Nat Rev Neurosci* **18**(2): 115-126.

Rubinov, M. and O. Sporns (2010), "Complex network measures of brain connectivity: uses and interpretations." *Neuroimage* **52**(3): 1059-1069.

Satterthwaite, T. D., R. Ciric, D. R. Roalf, C. Davatzikos, D. S. Bassett and D. H. Wolf (2019), "Motion artifact in studies of functional connectivity: Characteristics and mitigation strategies." *Hum Brain Mapp* **40**(7): 2033-2051.

Schlesinger, K. J., B. O. Turner, S. T. Grafton, M. B. Miller and J. M. Carlson (2017a), "Improving resolution of dynamic communities in human brain networks through targeted node removal." *PLoS One* **12**(12): e0187715.

Schlesinger, K. J., B. O. Turner, B. A. Lopez, M. B. Miller and J. M. Carlson (2017b), "Age-dependent changes in task-based modular organization of the human brain." *Neuroimage* **146**: 741-762.

Shao, J., Z. Dai, R. Zhu, X. Wang, S. Tao, K. Bi, S. Tian, H. Wang, Y. Sun, Z. Yao and Q. Lu (2019), "Early identification of bipolar from unipolar depression before manic episode: Evidence from dynamic rfMRI." *Bipolar Disord* **21**(8): 774-784.

Shine, J. M., O. Koyejo and R. A. Poldrack (2016), "Temporal metastates are associated with differential patterns of time-resolved connectivity, network topology, and attention." *Proc Natl Acad Sci U S A* **113**(35): 9888-9891.

Sonkusare, S., M. Breakspear and C. Guo (2019), "Naturalistic Stimuli in Neuroscience: Critically Acclaimed." *Trends Cogn Sci* **23**(8): 699-714.

Sporns, O. (2013), "Structure and function of complex brain networks." *Dialogues Clin Neurosci* **15**(3): 247-262.

Sporns, O. and R. F. Betzel (2016), "Modular Brain Networks." *Annu Rev Psychol* **67**: 613-640.

Telesford, Q. K., A. Ashourvan, N. F. Wymbs, S. T. Grafton, J. M. Vettel and D. S. Bassett (2017), "Cohesive network reconfiguration accompanies extended training." *Hum Brain Mapp* **38**(9): 4744-4759.

Telesford, Q. K., M. E. Lynall, J. Vettel, M. B. Miller, S. T. Grafton and D. S. Bassett (2016), "Detection of functional brain network reconfiguration during task-driven cognitive states." *Neuroimage* **142**: 198-210.

Tian, S., Y. Sun, J. Shao, S. Zhang, Z. Mo, X. Liu, Q. Wang, L. Wang, P. Zhao, M. R. Chattun, Z. Yao, T. Si and Q. Lu (2019), "Predicting escitalopram monotherapy response in depression: The role of anterior cingulate cortex." *Hum Brain Mapp*.

Tomasi, D. G., E. Shokri-Kojori and N. D. Volkow (2017), "Temporal Evolution of Brain Functional Connectivity Metrics: Could 7 Min of Rest be Enough?" *Cereb Cortex* **27**(8): 4153-4165.

Van Dijk, K. R., T. Hedden, A. Venkataraman, K. C. Evans, S. W. Lazar and R. L. Buckner (2010), "Intrinsic functional connectivity as a tool for human connectomics: theory, properties, and optimization." *J Neurophysiol* **103**(1): 297-321.

Vanderwal, T., J. Eilbott and F. X. Castellanos (2019), "Movies in the magnet: Naturalistic paradigms in developmental functional neuroimaging." *Dev Cogn Neurosci* **36**: 100600.

Vanderwal, T., J. Eilbott, E. S. Finn, R. C. Craddock, A. Turnbull and F. X. Castellanos (2017), "Individual differences in functional connectivity during naturalistic viewing conditions." *Neuroimage* **157**: 521-530.

Vanderwal, T., C. Kelly, J. Eilbott, L. C. Mayes and F. X. Castellanos (2015), "Inscapes: A movie paradigm to improve compliance in functional magnetic resonance imaging." *Neuroimage* **122**: 222-232.

Vohryzek, J., A. Griffa, E. Mullier, C. Friedrichs-Maeder, C. Sandini, M. Schaer, S. Eliez and P. Hgmann (2019), "Dynamic spatiotemporal patterns of brain connectivity reorganize across development." *Network Neuroscience*.

Voss, M. W., C. N. Wong, P. L. Baniqued, J. H. Burdette, K. I. Erickson, R. S. Prakash, E. McAuley, P. J. Laurienti and A. F. Kramer (2013), "Aging brain from a network science perspective: something to be positive about?" *PLoS One* **8**(11): e78345.

Wang, J., Y. Ren, X. Hu, V. T. Nguyen, L. Guo, J. Han and C. C. Guo (2017), "Test-retest reliability of functional connectivity networks during naturalistic fMRI paradigms." *Hum Brain Mapp* **38**(4): 2226-2241.

Watts, D. J. and S. H. Strogatz (1998), "Collective dynamics of 'small-world' networks." *Nature* **393**(6684): 440-442.

Wei, M., J. Qin, R. Yan, K. Bi, C. Liu, Z. Yao and Q. Lu (2017), "Abnormal dynamic community structure of the salience network in depression." *J Magn Reson Imaging* **45**(4): 1135-1143.

Weir, W. H., S. Emmons, R. Gibson, D. Taylor and P. J. Mucha (2017), "Post-Processing Partitions to Identify Domains of Modularity Optimization." *Algorithms* **10**(3).

Wymbs, N. F., D. S. Bassett, P. J. Mucha, M. A. Porter and S. T. Grafton (2012), "Differential recruitment of the sensorimotor putamen and frontoparietal cortex during motor chunking in humans." *Neuron* **74**(5): 936-946.

Xia, M., J. Wang and Y. He (2013), "BrainNet Viewer: a network visualization tool for human brain connectomics." *PLoS One* **8**(7): e68910.

Xu, T., A. Opitz, R. C. Craddock, M. J. Wright, X. N. Zuo and M. P. Milham (2016), "Assessing Variations in Areal Organization for the Intrinsic Brain: From Fingerprints to Reliability." *Cereb Cortex*.

Yan, C. G., B. Cheung, C. Kelly, S. Colcombe, R. C. Craddock, A. Di Martino, Q. Li, X. N. Zuo, F. X. Castellanos and M. P. Milham (2013), "A comprehensive assessment of regional variation in the impact of head micromovements on functional connectomics." *Neuroimage* **76**: 183-201.

Yan, C. G., Z. Yang, S. Colcombe and M. Milham (2017), "Concordance among indices of intrinsic brain function: Insights from inter-individual variation and temporal dynamics." *Science Bulletin* **62**(23): 1572-1584.

Yang, Z., R. C. Craddock, D. S. Margulies, C. G. Yan and M. P. Milham (2014), "Common intrinsic connectivity states among posteromedial cortex subdivisions: Insights from analysis of temporal dynamics." *Neuroimage* **93 Pt 1**: 124-137.

Yeo, B. T., F. M. Krienen, J. Sepulcre, M. R. Sabuncu, D. Lashkari, M. Hollinshead, J. L. Roffman, J. W. Smoller, L. Zollei, J. R. Polimeni, B. Fischl, H. Liu and R. L. Buckner (2011), "The organization of the human cerebral cortex estimated by intrinsic functional connectivity." *J Neurophysiol* **106**(3): 1125-1165.

Yu, M., K. A. Linn, P. A. Cook, M. L. Phillips, M. McInnis, M. Fava, M. H. Trivedi, M. M. Weissman, R. T. Shinohara and Y. I. Sheline (2018), "Statistical harmonization corrects site effects in functional connectivity measurements from multi-site fMRI data." *Hum Brain Mapp* **39**(11): 4213-4227.

Zhang, H., N. Stanley, P. J. Mucha, W. Yin, W. Lin and D. Shen (2018). Multi-layer large-scale functional connectome reveals infant brain development patterns. International Conference on Medical Image Computing and Computer Assisted Intervention, Granada, Spain, Springer.

Zhang, Z., Q. K. Telesford, C. Giusti, K. O. Lim and D. S. Bassett (2016), "Choosing Wavelet Methods, Filters, and Lengths for Functional Brain Network Construction." *PLoS One* **11**(6): e0157243.

Zheng, H., F. Li, Q. Bo, X. Li, L. Yao, Z. Yao, C. Wang and X. Wu (2018), "The dynamic characteristics of the anterior cingulate cortex in resting-state fMRI of patients with depression." *J Affect Disord* **227**: 391-397.

Zuo, X. N. and X. X. Xing (2014), "Test-retest reliabilities of resting-state FMRI measurements in human brain functional connectomics: a systems neuroscience perspective." *Neurosci Biobehav Rev* **45**: 100-118.

Zuo, X. N., T. Xu, L. Jiang, Z. Yang, X. Y. Cao, Y. He, Y. F. Zang, F. X. Castellanos and M. P. Milham (2013), "Toward reliable characterization of functional homogeneity in the human brain: preprocessing, scan duration, imaging resolution and computational space." *Neuroimage* **65**: 374-386.

Zuo, X. N., T. Xu and M. P. Milham (2019), "Harnessing reliability for neuroscience research." *Nat Hum Behav* **3**(8): 768-771.

Supplementary Materials

Methods

Human Connectome Project (HCP)

The original retest dataset included 45 subjects with imaging data (https://www.humanconnectome.org/study/hcp-young-adult/data-releases). Each subject had four resting state fMRI runs collected using the same protocol on a 3T Siemens Skyra with a multiband gradient-echo EPI sequence (multiband factor=8, TR=0.72 s, echo time = 33.1 ms, field of view = 208 × 180 mm^2, number of slices = 72, voxel size = 2 mm^3, and flip angle = 52°). All subjects are monozygotic twins (19 twin pairs and 7 without a paired twin). Three subjects were excluded due to incomplete data acquisition (total number of volumes less than 80%). For the remaining 42 subjects (16 twin pairs and 10 without a paired twin), one subject from each twin pair (the one who is more right-handed and/or with a test-retest interval closer to the median was chosen). Only one subject from a twin pair was included to avoid the twin-related decrease in between-subject variance. Additionally, one nonpaired twin who is left-handed was excluded, leaving a total number of 25 right-handed subjects for analysis (age: 22 to 35 years, 9 males/16 females, test-retest intervals ranging from 52 to 326 days).

Functional imaging preprocessing used HCP functional and ICA-Fix pipelines. The functional pipeline includes gradient distortion correction, motion correction, field bias correction, spatial registration into a common Montreal Neurological Institute (MNI) space, intensity normalization (Glasser et al. 2013), and artifact removal using independent component analysis FIX (Griffanti et al. 2014, Salimi-Khorshidi et al. 2014). After preprocessing, flexibility across the $\gamma-\omega$ plane and the intra-class correlation coefficient (ICC) of flexibility were computed in the same way as in the HBN-SSI data. The window length was 139 TRs (~100 s) which is comparable to that used for the HBN-SSI dataset.

Toy Data

To test the impact of GenLouvain code implementation on recovering known underlying dynamic changes in community structure, we created a toy multilayer network dataset. It consists of 128 nodes which were divided into four 32-node communities where each community represents a complete graph (i.e., all nodes are interconnected with each other). Across 13 layers, these four communities either split to form a 16-node community or merge to form a 32-node community. As shown in **Figure S3A**, the four communities split or merge at different rates; Community 1 does not change, Community 2 splits or merges every three layers, Community 3 splits or merges every two layers, and Community 4 splits or merges every layer. The changes in community structure across layers (over time) can be captured using the GenLouvain algorithm (**Figure S3B**). Whenever the community assignment of a node changes, this fact is recorded and can be used to calculate node flexibility; as shown in **Figure S3C**, node flexibility varies across nodes in the four original communities, with nodes originally in Community 1 showing no changes and nodes originally in Community 4 showing the most changes.

Given that output from the GenLouvain algorithm is nondeterministic, it is common practice to run the algorithm across multiple optimizations. In the case of the toy network, after 1000 optimizations, a change should occur with a 50% probability at each split or merge. This behavior occurs because all edges in the network have equal weight, and thus when a 32-node community splits, there is equal likelihood that nodes forming the new community come from either set of 16 nodes. Likewise, when a community merges, there is equal likelihood that the older community will cease and join the new community, or the newer community will cease and return to the older community.

Figure legends

Figure S1. The impact of the GenLouvain method (‘*moverandw*’ vs. ‘*move*’) on dynamic network measures. In the 2-dimensional γ–ω parameter space, abrupt changes in flexibility, integration, and recruitment were observed when the method ‘*move*’ was used **(A)**. This issue is most serious for flexibility, followed by integration, and less so for recruitment. The method ‘*moverandw*’ mitigates this issue and results in an apparently more continuous landscape **(B).** Reliability between the two methods above the point of apparent discontinuity is close to zero for flexibility, ranges from low to medium for integration, and ranges from low to high for recruitment (**C**).

Figure S2. Test-retest reliability of dynamic network measures was substantially impacted by the GenLouvain method. The test-retest reliability in the portion of the parameter space above the apparent discontinuity is lower for ‘*move*’ (**A**) compared to ‘*moverandw*’ (**B**) for flexibility, integration, and recruitment. Results were obtained for the movie condition with 60 minutes of data.

Figure S3. The impact of the GenLouvain method (‘*moverandw*’ vs. ‘*move*’) on multilayer network analyses in the toy data. (**A**) A multilayer network representing groups of nodes split into four communities shows the splitting and merging of communities across 13 layers. (**B**) Community structure across layers is identified by the GenLouvain algorithm (we show one optimization here). (**C**) Node flexibility quantifies how often a node changes community assignment. From the single optimization, flexibility is calculated by finding the number of times a node changes community divided by the number of possible times the nodes can change. In practice, flexibility is calculated across multiple optimizations. Using the GenLouvain algorithm across n = 1000 optimizations, it is expected that at the point where a community changes, there is a 50% chance that a group of nodes will form the new community or merge with an old community. When comparing method choice, it is readily apparent that although results appear visually similar at one optimization, the '*move*' method (**D**) does not result in community changes with equal likelihood at each split or merge, while using the '*moverandw*' (**E**) method produces the expected outcome for this toy network.

Figure S4. The method '*moverandw*' performs better than '*move*' in terms of recovering the underlying dynamic changes in modular structure regardless of the γ−ω selection. When using the GenLouvain algorithm, the parameters γ and ω change the average flexibility measured across nodes. (**A**) In comparing the algorithms, we noticed that using the method '*move*' results in values of the dynamic network metric that abruptly drop off at ω values greater than 1. Using the newer method '*moverandw*' does not produce this abrupt change, resulting in an apparently more continuous modulation of the metric values. (**B**) Although the values in the parameter space appear similar below the apparent discontinuity seen using '*move*', multiple optimizations reveal stark differences in the converging results. When choosing a value below the apparent discontinuity (γ = 1.00, ω = 0.25), the output from '*moverandw*' matches the expected outcome for the toy network. In contrast, '*move*' does not produce the expected outcome. When choosing a value above the apparent discontinuity, '*moverandw*' is still able to recover the expected outcome while '*move*' does not find any changes.

Figure S5. Comparison of our parameter selection [γ=1.05, ω=2.5] and previously recommended parameters [γ=1, ω=1]. The spatial topographies of mean flexibility computed across subjects for

two parameter choices are similar (**A**: Pearson's r=0.70), even though the range of flexibility values differs. Consistent with previous work (Betzel et al. 2017), we found that high-order cognitive regions had greater flexibility than primary cortices. For the movie condition, visual cortex had the lowest flexibility. Compared to the parameter choice [γ=1, ω=1], [γ=1.05, ω=2.5] had much higher test-retest reliability across the brain (except for visual cortex) (**B**). The low test-retest reliability of flexibility observed at [γ=1, ω=1] is driven by low between-subject variance (Between-Sub-Var: **C**) and high within-subject variance (Within-Sub Var: **D**). The relatively low ICCs (although still medium in size) observed in visual cortex at [γ=1.05, ω=2.5] are associated with comparable within- and between-subject variance. In the scatter plot, each dot represents an ROI. These results were obtained based on the movie condition using 60 minutes of data.

Figure S6. HBN-SSI and HCP data differed in flexibility values and the test-retest reliability of flexibility across the γ−ω plane. Using 60 min of resting state data, flexibility (**A**) and ICC of flexibility (**B**) were computed in the same way for HBN-SSI and HCP data. In HBN-SSI data, there was a range of parameters with high reliability (ICC≥0.6). However, in HCP data, we were unable to find a range of reliability-optimized parameters. Overall, the flexibility across the γ−ω landscape was lower for HCP than for HBN-SSI data.

Figure S7. Regional and system-level variations in reliability improvement as a function of scan duration for the movie condition. (**A**) The ICC values were plotted on the brain's surface for flexibility, integration, and recruitment at six scan durations. For ease of interpretation, regional ICC values were summarized using Yeo et al. (2011)'s seven networks for three measures (flexibility: **B**; integration: **C**; and recruitment: **D**) and each of the six scan durations. With 10 min of data, ICC values of dynamic metrics were low in all networks, except for recruitment in the visual network. With increased scan duration, reliability of dynamic metrics improved, and the improvement was most noticeable from 10 to 20 min. The visual network had the lowest reliability for flexibility and highest reliability for recruitment. Spatial variation was less obvious for integration than for the other two measures.

Figure S8. For the flanker task, dynamic network measures were more reliable when estimated from the low frequency components of the fMRI signal (0.01-0.1Hz) compared to the high frequency components (0.1-0.3Hz). ICCs of the 200 ROIs were plotted on the brain surface and summarized in a violin plot for low (red) and high (blue) frequency components of the fMRI signal.

Supplementary Figures

Figure S1

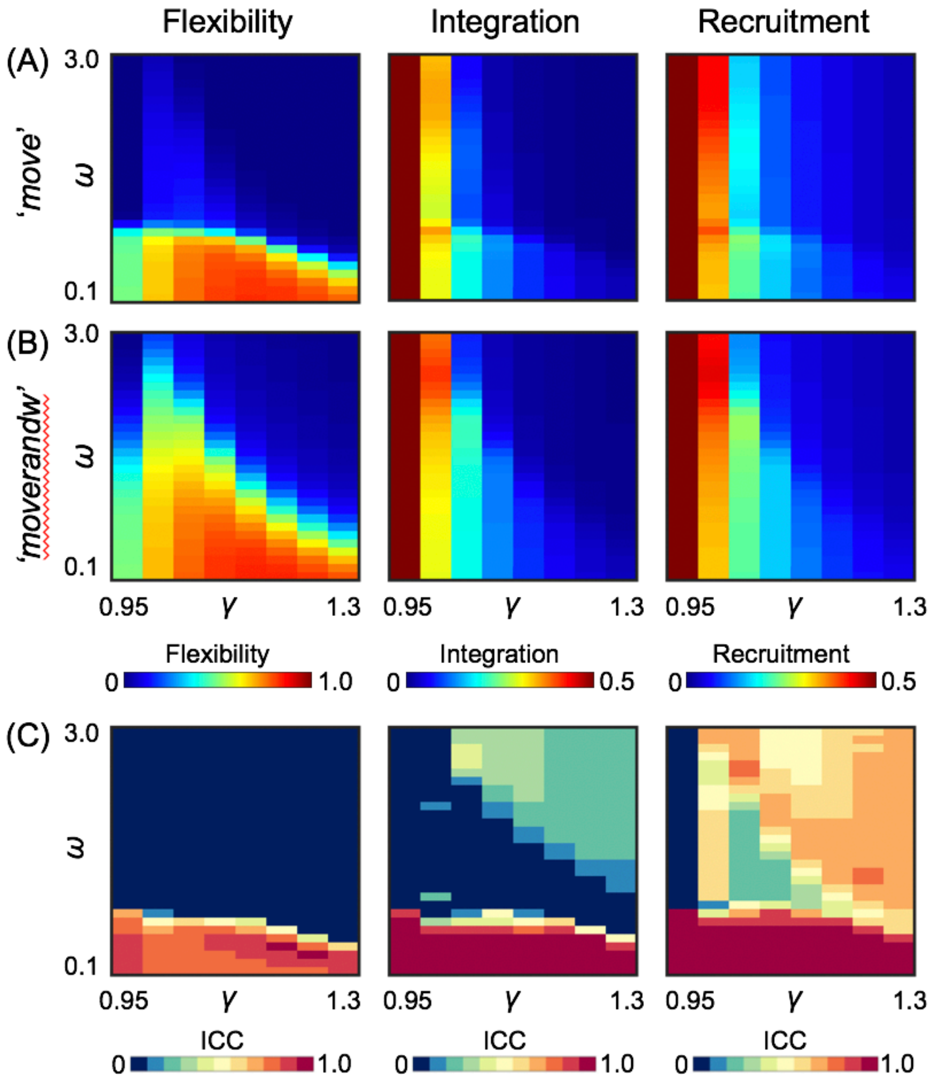

Figure S2

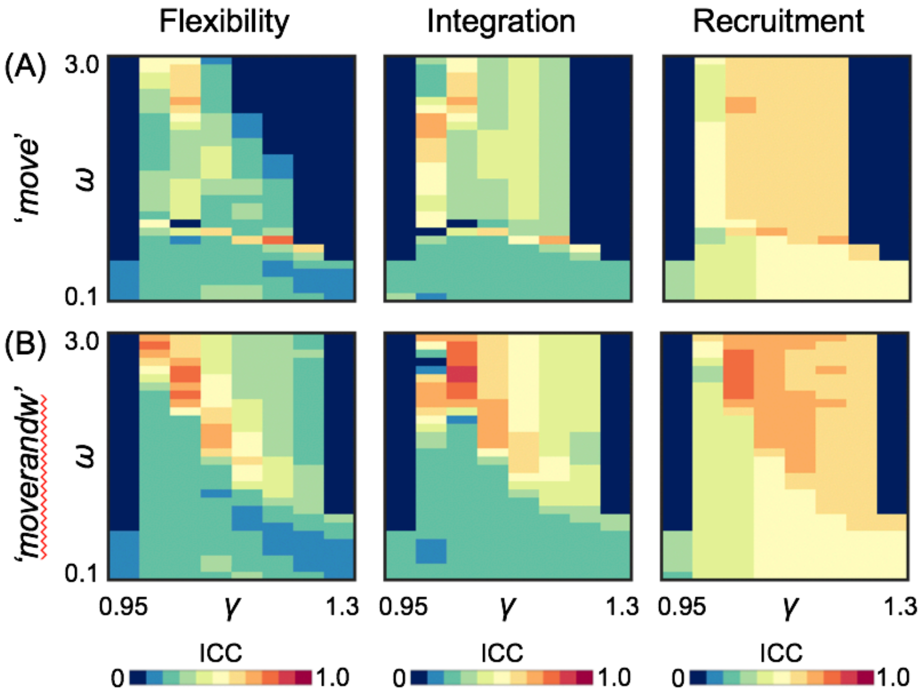
Flexibility
Integration
Recruitment
(A)
'move'
(B)
'moverandw'
3.0
ω
0.1
0.95
γ
1.3
ICC
0
1.0

Figure S3

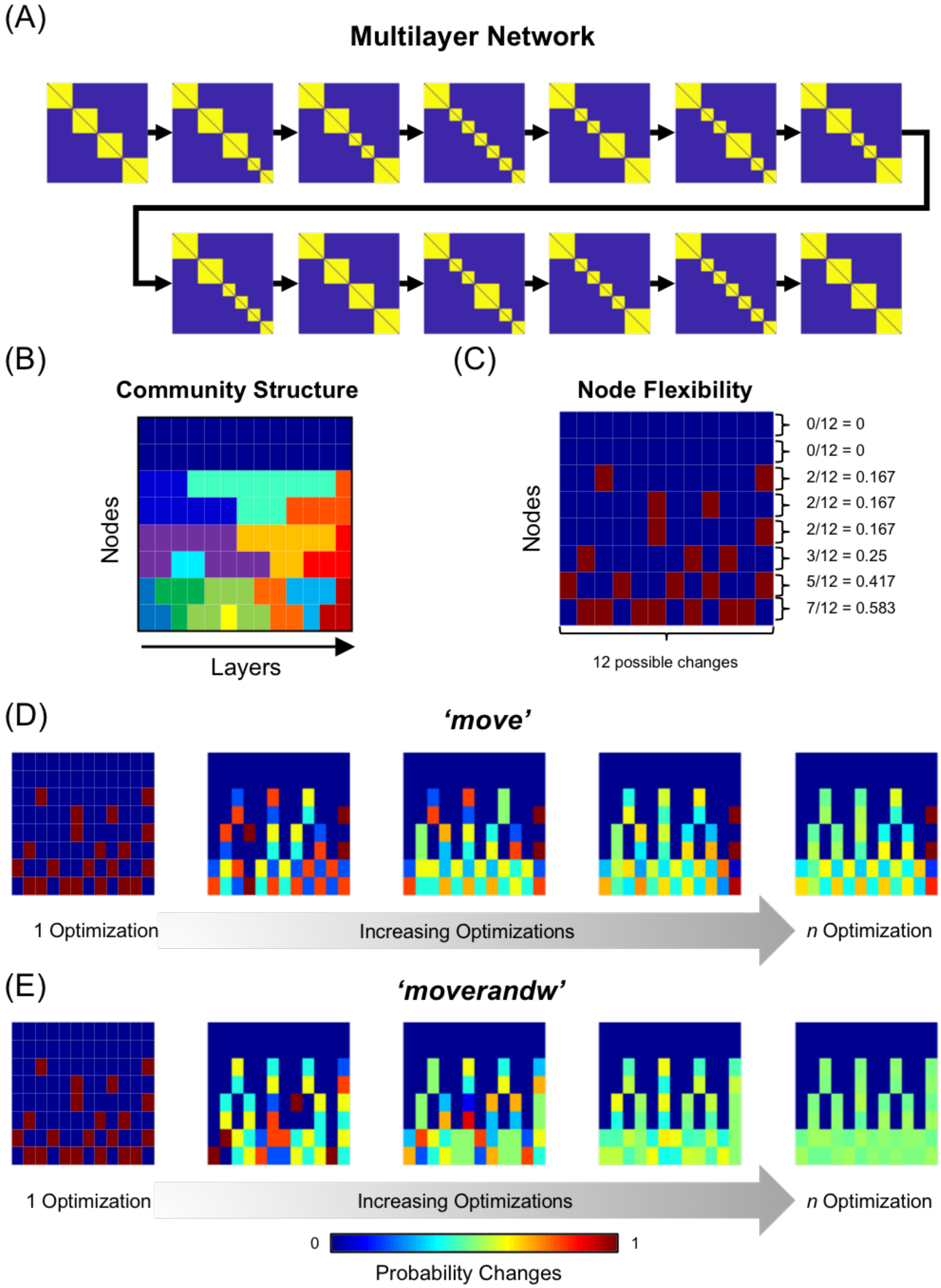
(A)
Multilayer Network
(B)
Community Structure
Nodes
Layers
(C)
Node Flexibility
Nodes
0/12 = 0
0/12 = 0
2/12 = 0.167
2/12 = 0.167
2/12 = 0.167
3/12 = 0.25
5/12 = 0.417
7/12 = 0.583
12 possible changes
(D)
'move'
1 Optimization
Increasing Optimizations
n Optimization
(E)
'moverandw'
1 Optimization
Increasing Optimizations
n Optimization
0
1
Probability Changes

Figure S4

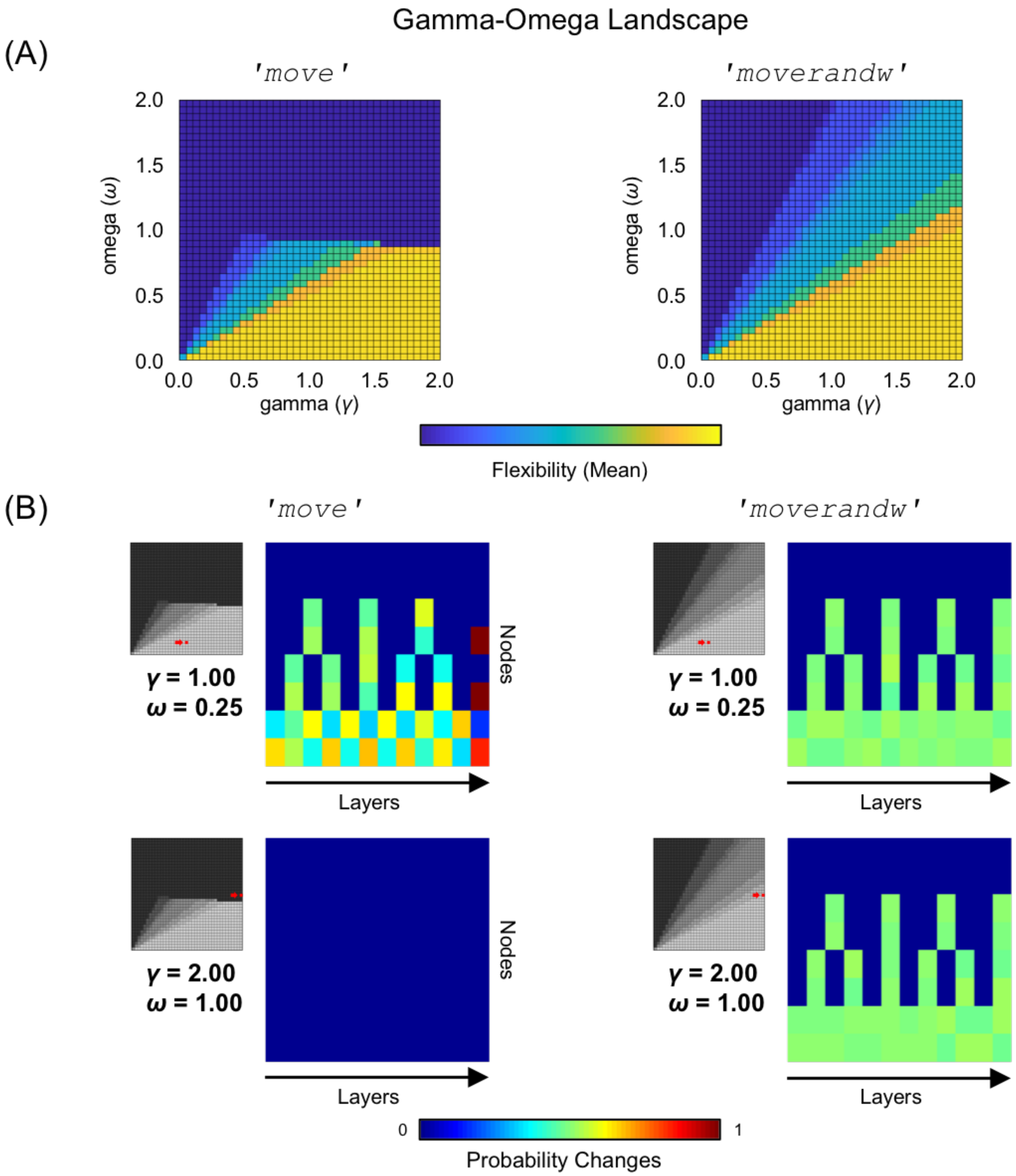
Gamma-Omega Landscape
(A)
'move'
'moverandw'
2.0
1.5
1.0
0.5
0.0
omega (ω)
0.0
0.5
1.0
1.5
2.0
gamma (γ)
Flexibility (Mean)
(B)
'move'
'moverandw'
γ = 1.00
ω = 0.25
γ = 2.00
ω = 1.00
Nodes
Layers
0
1
Probability Changes

Figure S5

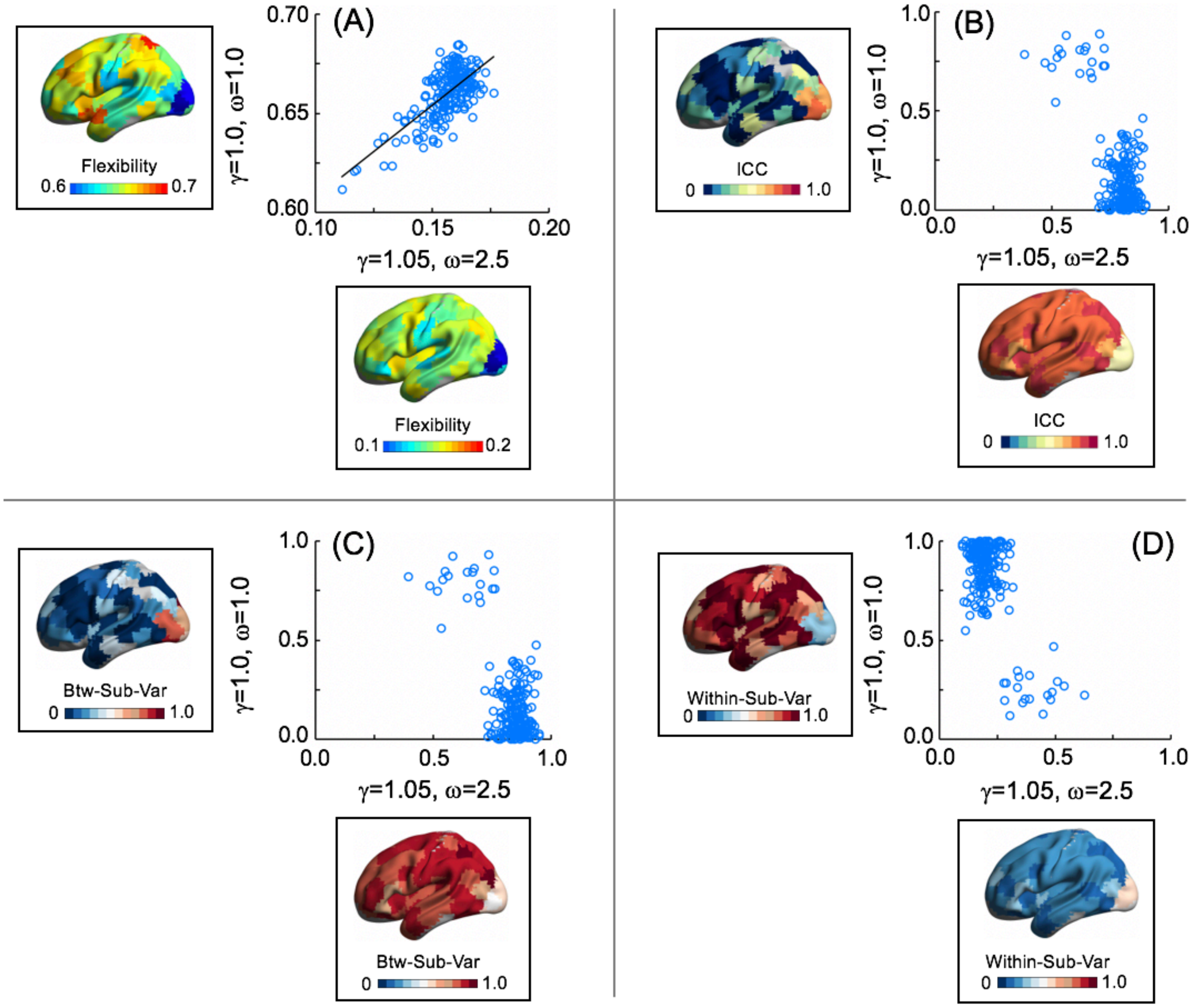
(A)
Flexibility
0.6
0.7
0.70
0.65
0.60
0.10
0.15
0.20
γ=1.0, ω=1.0
γ=1.05, ω=2.5
Flexibility
0.1
0.2
(B)
ICC
0
1.0
0.0
0.5
1.0
γ=1.0, ω=1.0
γ=1.05, ω=2.5
ICC
0
1.0
(C)
Btw-Sub-Var
0
1.0
0.0
0.5
1.0
γ=1.0, ω=1.0
γ=1.05, ω=2.5
Btw-Sub-Var
0
1.0
(D)
Within-Sub-Var
0
1.0
0.0
0.5
1.0
γ=1.0, ω=1.0
γ=1.05, ω=2.5
Within-Sub-Var
0
1.0

Figure S6

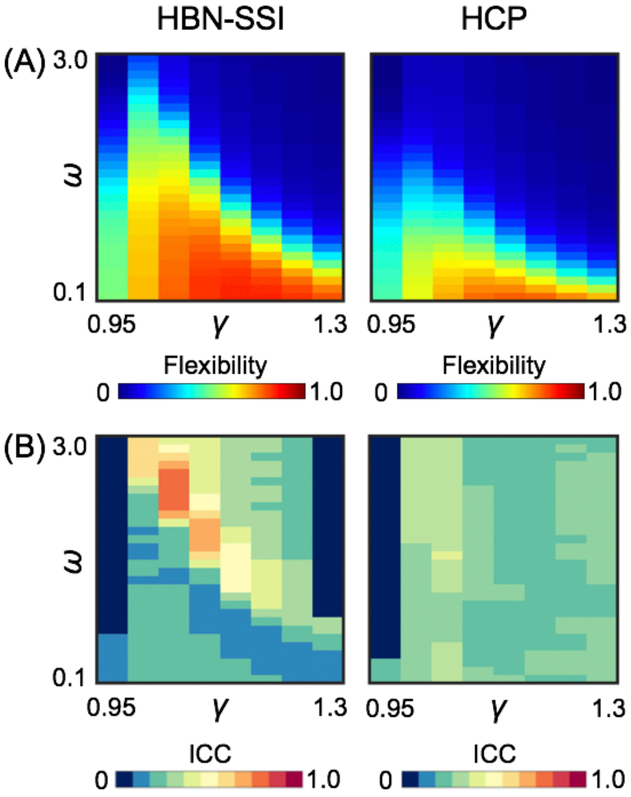

Figure S7

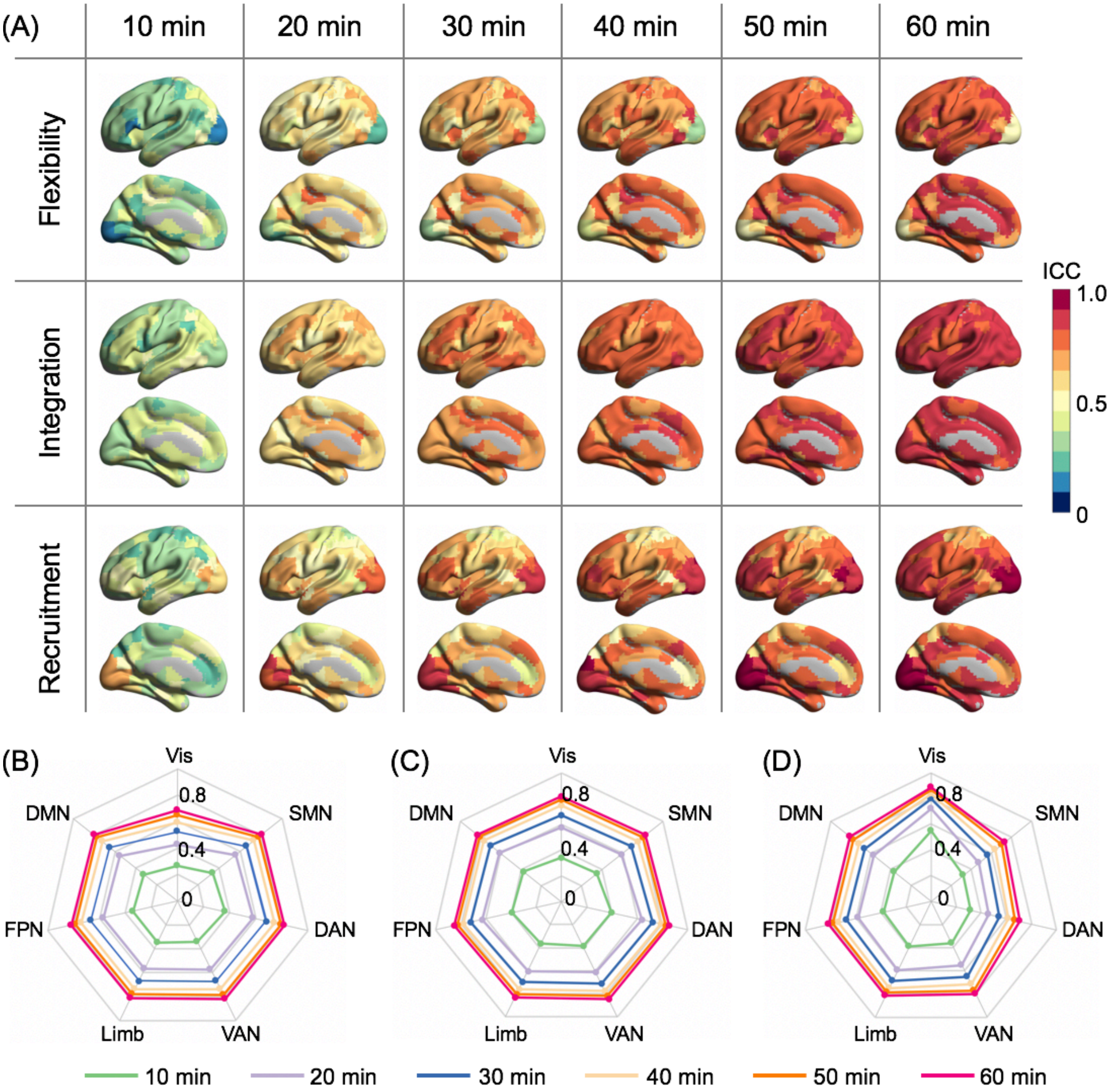
(A)
10 min
20 min
30 min
40 min
50 min
60 min
Flexibility
Integration
Recruitment
ICC
1.0
0.5
0
(B)
(C)
(D)
Vis
SMN
DAN
VAN
Limb
FPN
DMN
0.8
0.4
0
10 min
20 min
30 min
40 min
50 min
60 min

Figure S8

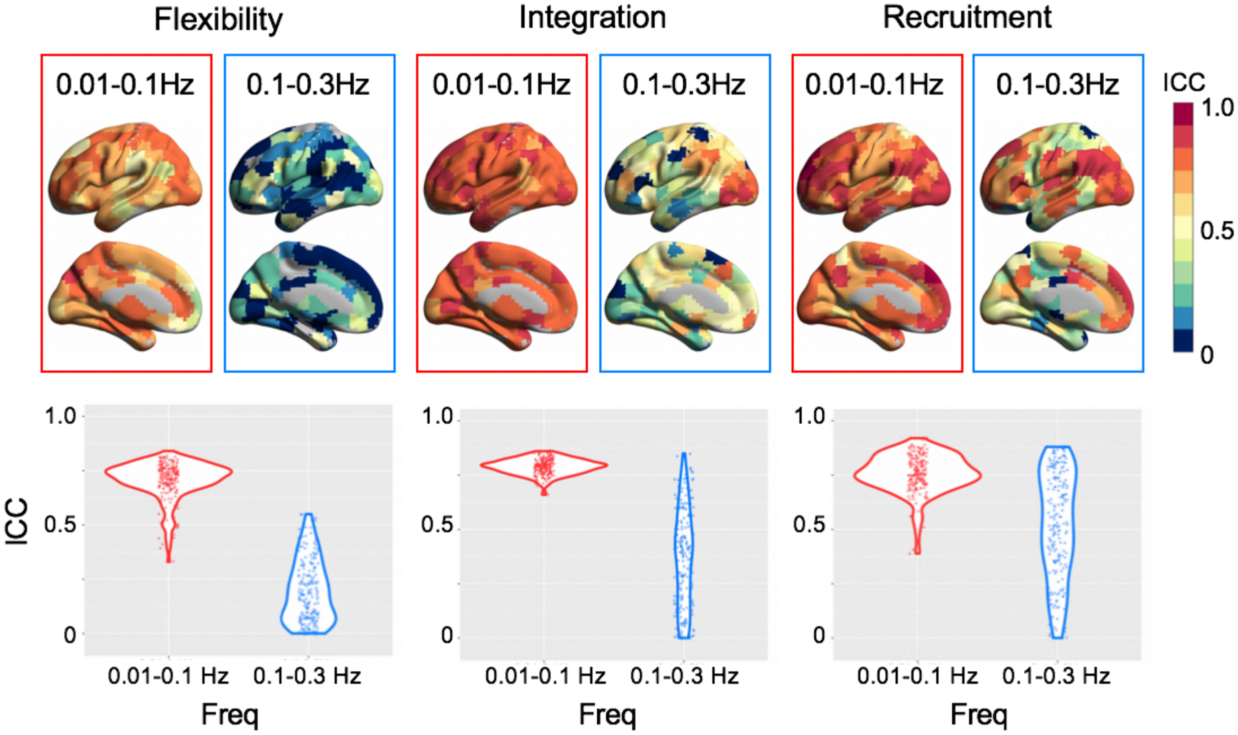
Flexibility
Integration
Recruitment
0.01-0.1Hz
0.1-0.3Hz
0.01-0.1Hz
0.1-0.3Hz
0.01-0.1Hz
0.1-0.3Hz
ICC
1.0
0.5
0
ICC
1.0
0.5
0
0.01-0.1 Hz
0.1-0.3 Hz
Freq

References

Betzel, R. F., T. D. Satterthwaite, J. I. Gold and D. S. Bassett (2017), "Positive affect, surprise, and fatigue are correlates of network flexibility." *Sci Rep* **7**(1): 520.

Glasser, M. F., S. N. Sotiropoulos, J. A. Wilson, T. S. Coalson, B. Fischl, J. L. Andersson, J. Xu, S. Jbabdi, M. Webster, J. R. Polimeni, D. C. Van Essen, M. Jenkinson and W. U.-M. H. Consortium (2013), "The minimal preprocessing pipelines for the Human Connectome Project." *Neuroimage* **80**: 105-124.

Griffanti, L., G. Salimi-Khorshidi, C. F. Beckmann, E. J. Auerbach, G. Douaud, C. E. Sexton, E. Zsoldos, K. P. Ebmeier, N. Filippini, C. E. Mackay, S. Moeller, J. Xu, E. Yacoub, G. Baselli, K. Ugurbil, K. L. Miller and S. M. Smith (2014), "ICA-based artefact removal and accelerated fMRI acquisition for improved resting state network imaging." *Neuroimage* **95**: 232-247.

Salimi-Khorshidi, G., G. Douaud, C. F. Beckmann, M. F. Glasser, L. Griffanti and S. M. Smith (2014), "Automatic denoising of functional MRI data: combining independent component analysis and hierarchical fusion of classifiers." *Neuroimage* **90**: 449-468.